UNIVERSITÀ DI PISA
Facoltà di Ingegneria

Corso di Laurea Magistrale in Ingegneria Biomedica

TESI DI LAUREA

Study and development of stretchable sensors for flexible surgical instrumentation

Candidato:
Stefania Russo

Relatori:
Prof.ssa Arianna Menciassi
Ing. Tommaso Ranzani

Anno accademico 2013/2014

Summary

CHAPTER 1: BACKGROUND

1.1 Minimally invasive surgery: state of the art

The field of surgery is under constant evolution, helped by new diagnostic and therapeutic strategies and thanks to the advent of antibiotics and anaesthetics that make procedures more safe and effective, improving clinical outcome.

A turning point in surgery was the development of the rod-lens endoscope [1], an instrument used to examine the interior of a hollow organ or cavity of the body to diagnose, monitor, and surgically treat various medical problems.

All of these technological advancements in surgery have resulted in the outcome of a minimally invasive medical procedure. In minimally invasive surgery (MIS), surgical procedures are carried out trying to minimize the access trauma through small incisions using different access routes to the target operative anatomy with extraluminal, intraluminal and transluminal approaches, as shown in Figure 1.

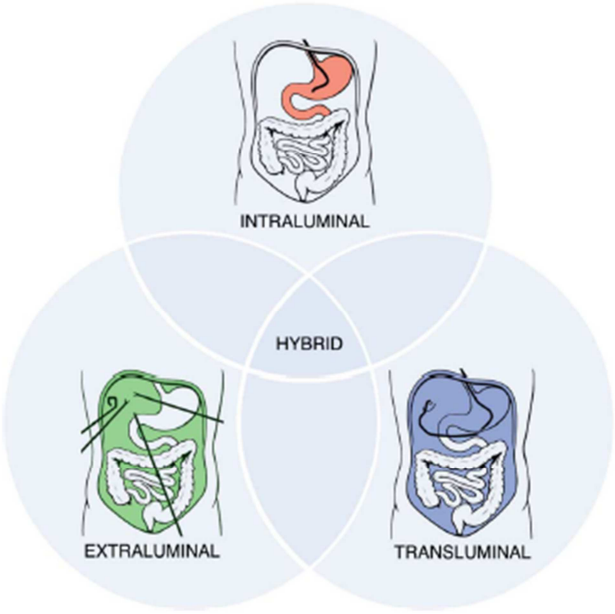

Figure 1. Classification of MIS procedures based on the access routes to the target operative anatomy [2]

Laparoscopy is an example of extraluminal access by passage of rigid instruments via small incisions; this can be performed also through a single entry point, typically the patient's navel, in the called laparo-endoscopic single-site surgery (LESS) or single-port laparoscopy (SPL).

Intraluminal procedures are performed through tubular anatomical structures directly exploiting natural orifices. Transluminal approach is provided via a breach of this luminal barrier for entrering to body cavities such as the abdomen [2].

Since the entry incisions are smaller with respect to open surgery, patients tend to have quicker recovery times, less discomfort due to the reduced trauma and improved cosmetic than with conventional open surgery [3].

Figure 2. Progress and status of research: some of the key milestones in minimally invasive surgery

As mentioned above, laparoscopy is an example of MIS and it involves use of devices and remote-control manipulation of instruments with indirect observation of the surgical field through an endoscope.
In MIS laparoscopic procedures, the surgeon usually makes small incisions in the patient's skin through which the operating tools and a camera are inserted. The abdomen is inflated with carbon dioxide gas. This lifts up the abdominal wall to create an adequate working and viewing space. CO_2 is used since it can be absorbed by tissue and removed by the respiratory system [4].
The surgeon then views the operating site, usually on a monitor, while controlling the tools. Despite this, minimally invasive surgeries have their challenges: the rigid instruments used are typically more than 30 centimetres long—which amplify a surgeon's normal hand tremor. This rigidity also results in the inability to articulate their end effectors, therefore in the lack of the degrees of freedom (DoFs) needed in certain situations [5]. In addition, surgeons must deal with what's known as the fulcrum effect: when the hand moves to the right, the tip of the surgical instrument moves to the left, thus affecting considerably the intuitiveness of the procedure: laparoscopy surgery requires extensive operating skills and training for the surgeon [6], who still has limited dexterity, flexibility and manoeuvrability of the available tools.

1.2 Robots in surgery

As shown in Figure 2, robots have been introduced into operating rooms in order to overcome some of the limitations in the instrumentation used in minimally invasive procedures. A relevant example consists in the da Vinci surgical system, introduced in 1999 by Intuitive Surgical of Sunnyvale, CA [7]. The first generation of the da Vinci consists of a surgeon's console that is in the same room of the patient, and a patient-side cart with three interactive robotic arms.
The surgeon sits at the console and looks at a 3D image of the procedure and, thanks to a joystick-like controls located beneath the screen, he is able to tele-operate the arms of the robot. Indeed the system translates the surgeon's hand, wrist and finger movements into real-time movements of surgical instruments. The fulcrum effect is compensated via software. At the same time, tremor removal and motion scaling allow accurate and precise motion control of the instrument tip. The primary advantage of the system is that it not only restores the wrist articulation lost during conventional laparoscopy, but the instruments are designed with seven DoF, a range of motion even greater than the human wrist [6].
The patient-side cart is where the patient is positioned during surgery. It includes three robotic arms that carry out the surgeon's commands.

The system is equipped with a high-definition endoscope composed of a flexible tube with a camera and light at the tip and image processing equipment.
The vision cart is a large monitor that provides the surgical assistant at the patient's side a view of the operating field.
Other systems have been developed over the years (e.g. the da Vinci S HD Surgical System, or the da Vinci Si Surgical System) with improvements of the vision system and of the user interface, dual-console capability to support training and collaboration during surgery and increased number of the robotic arms (from three to four).

Figure 3. Overview of the Da Vinci Surgical System [7]: on the left the surgeon console is shown; on the right the patient cart with three instrument arms and the vision cart are illustrated.

With 620 da Vinci sold in the year 2012 and more than 2400 systems installed at nearly 2000 hospitals worldwide, the system is now used in about 80% of prostatectomies in the United States, and the worldwide procedures grew by approximately 25% year over year [6, 8].
But such surgical robots also have their problems that go from the costs (more than US $1 million), to the size and weight—about 180 centimetres tall and more than 900 kilograms. This means the necessity of a large, equipped and dedicated operating room to integrate the system. And if a complication arises and the operation must be converted to an open surgery, it's difficult to move the robot out of the way quickly so the surgeon can step in.

1.3 NOTES and Single Port surgery

Recently, attention has been focused to minimize the invasiveness of the existing MIS approaches: transluminal surgery is introduced as an expansion of the intraluminal operations; this procedure is called natural orifice transluminal endoscopic surgery (NOTES) [2]. In NOTES, scarless abdominal operations can be performed with an endoscope passed through a natural orifice chosen according to the specific procedure to be performed.
This technique may introduce several advantages from the patient's perspective (pain reduction, short patient recovery time, and better aesthetics results) but it introduces lots of challenges for the physicians [9].
Especially here, the procedure is more complex because the use of rigid or semi-rigid tools may lead to significant clashing of the tools: furthermore the available instrumentation compatible with endoscopes is generally inadequate for these procedures because it cannot guarantee the required tissue dissection,

destruction and reconstruction capabilities. The design of specialized devices to allow navigation to the operative site while maintaining adequate stability and triangulation for tissue manipulation is therefore needed.
The use of flexible endoscopes has been investigated for achieving a good target-reaching, but they may lack in stability [10].
The goal is to meet the same capabilities of complex multihanded laparoscopic instruments and ideally the abilities of the human hands to perform open surgery. This could be accomplished by a platform design anthropomorphically inspired by the features of hands and eyes: based on the above considerations, various innovative endoluminal robotic platforms have been developed [2].
Up to now limited results have been obtained for NOTES because there are few robots (sophisticated and expensive) capable of navigating the complex anatomical geometry of a natural lumen [9].
Other drawbacks are the low patient acceptance, the necessity of a highly skilled multidisciplinary team and the lack of sterilizations combined with the risk of unsecure closure of internal incision in stomach or colon [11].
The SPL or SILS (Single Incision Laparoscopic Surgery) in another newly emerging technique in laparoscopy [11]; there are different names for SPL like SPA (Single Port Access) or LESS (LaparoEndoscopic Single-site Surgery). The whole surgery is conducted through a single incision: this means that is used a port containing multiple smaller internal cannulas through which up to four laparoscopic instruments may be inserted [2].
An examples of cholecystectomy performed with SILS is shown in Figure 4:

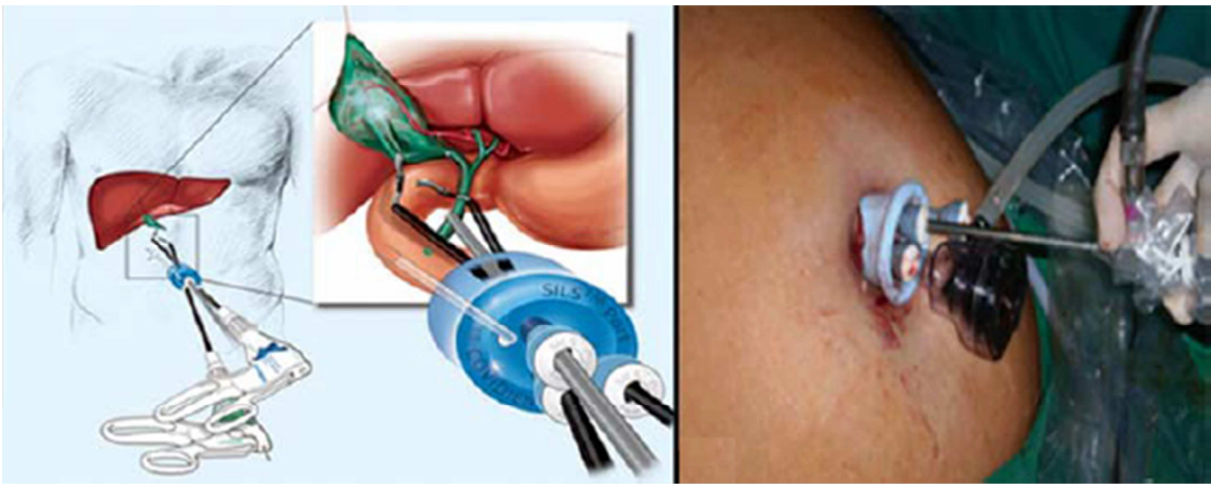

Figure 4. On the left the access port and the instruments are shown; on the right a view of the operation through the umbilicus [11].

In general LESS has the advantages of better cosmetics, less blood loss, better patient acceptance and easy tissue retrieval.
The critics are high costs, more chances of port site hernia and infections, inadequate triangulation, instrument crowding, and hands clashing.
To address these issues, curved instruments with different configurations have been developed. However, thus far dexterity has been introduced only at the handle or at the distal tip of the instruments, while the shaft remains rigid [2].
An example of robot performing SPL is the so called robotic laparoendoscopic single site surgery (R-LESS) using the da Vinci Single-Site VeSPA, based on software and instrument modifications of the SI system [12].

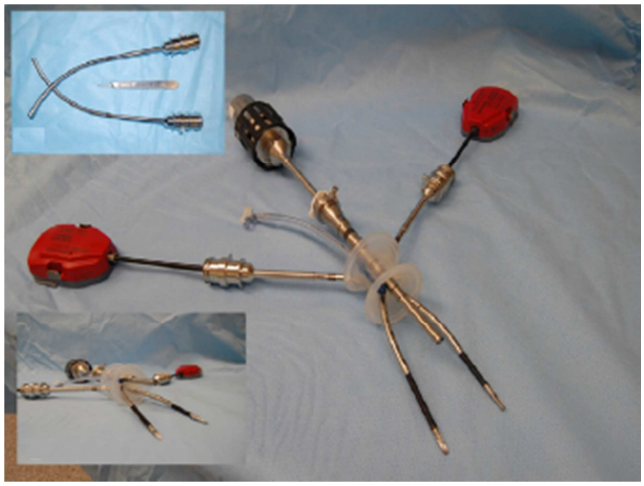

Figure 5. VeSPA instruments and accessories: curved cannulae and multichannel single-port, 8.5-mm robotic scope, flexible instruments passed through the cannulae

R-LESS appears to overcome some of the limitations encountered in conventional LESS, using curved instrument cannulae and semi rigid instruments (Figure 5) that avoid cannula collisions, arm interferences and port-site movement. Furthermore the da Vinci System software automatically detects and re-associates the user's hands with the instrument tips [13].
Although R-LESS continues to evolve, limitations are often meet, including a reduction in intracorporeal range of motion of the robotic instruments, extracorporeal instrument clashing and poor access for bedside assistance due to the robot size [12, 14].

1.4 Continuum-like robots

The term *flexible access surgery* most appropriately characterizes the novel techniques for the next evolutionary phase of MIS.
Today's challenge is to develop a technology that meets the demands of flexible access surgery. Thus, recent works have studied continuum like robots.
Traditional robots are heavy and stiff, because are mostly designed to work in manufacturing, featuring a structure inspired by that of the human arm, based on a serial arrangement of rigid links, connected by a relative small (six or fewer) degrees of freedom (DoF). They successfully perform a repetitively motion with great precision in industrial automation, but in surgical applications, where there is a need for highly dexterous yet reliable devices that have to be in contact with humans and with unstructured environments, robots with a stiff structure are insufficient to satisfy these needs [13]. In contrast, continuum robots exhibit higher dexterity and compliant contact. This has led to the development of continuum or hyper-redundant robots [15].
A continuum robot is a continuously curving manipulator; differently from robots with rigid links where motion occurs only in discrete locations (i.e. joints), a continuum robot has virtually an infinite number of DoFs allowing them the capability of work in unpredictable environment, but posing high challenges for designing, manufacturing, modelling and control. Also, in continuum robots the manipulation load is not necessarily placed at the end-effector, but due to their structure, whole-arm manipulation is possible, firmly grasping objects of different shapes and sizes using their entire length.
Potential applications of such robots span from people rescuing in narrow or hostile environment, to medical applications in minimally invasive surgery.
There is a great variety of continuum structures in nature, e.g., worms, snakes, elephant trunks, starfish tube feet, and octopus arms [16]; examples of soft bodied animals from which it is taken inspiration are worms, which achieve locomotion by creating traveling waves of contraction and expansion of their muscles; caterpillars are climbing animals exerting compressive forces on the substrate and controlling the release of body tension; cephalopods , in particular octopus mimic the environment and exhibit the ability

to manipulate objects, thanks to their arms, packed with muscles [17]. For these reasons these animals have become an inspiration for soft robotic arms and manipulators.
Several industrial robots inspired by these animals have been studied:

- Bionic Handling Assistant [18]: it is a compliant, pneumatically actuated continuum manipulator designed to be used for cooperative manipulation, copying an elephant's trunk [19], manufactured by *Festo* (http://www.festo.com/). The robot is made almost completely out of polyamide which makes it very flexible and lightweight (ca. 1.8kg). The robot comprises three main segments, each with three pneumatic bellow actuators, a ball-joint as wrist, also actuated by three actuators, and a three finger gripper actuated by one bellow actuator. When actuated, the robot can extend its length and can cause arc-like deformations. The overall length without actuation is 0,75m. Supplying full pressure on the actuators extends the overall length to 1.2m.
- OctArm is a continuum robot biologically-inspired by the octopus, capable of whole arm manipulation, biologically-inspired manoeuvring, and grasping abilities. It is comprised of four sections connected by endplates, providing twelve degrees of freedom. OctArm uses air muscle actuators that provide the large strength to weight ratio and strain required for soft robot manipulators [20].
- Snake Arm robot by *OC Robotics* (http://www.ocrobotics.com/) is specifically designed to perform remote handling operations in confined spaces; it has a long and flexible design allowing it to navigate through an open space, avoiding obstacles, carrying heavy tools and conducting work controlling its shape whit wire ropes that transfer mechanical power from the actuator pack into the snake-arm. These abilities are helpful in the nuclear industry with the problems of radiation dosage and limited spaces; the robot is well suited also for aircraft assembly, to develop aerospace robots capable of inspection, drilling, sealing and swaging, installation of components, laser welding, painting, removal of liquids, gases and thermal imaging.
  Snake-arm robot has also its advantages in hazardous situations: has been demonstrated the capability of the arm to reach a car through an open window and going under the steering wheel into the driver's footwell and inspecting the back seat of the car as well as underneath the car. Tip-mounted camera and lights provided the operator with remote views of the car.

As mentioned above, there are various disadvantages using heavy and stiff structures in surgery, as the da Vinci robot. Using an hyper-redundant robot could resolve these drawbacks because its continuous structure allow the necessary distal dexterity of surgical tools, therefore the availability of suitable DoFs and the small size necessary for complex operations in MIS [21]. Examples of highly articulated robots in surgery are:

- CardioARM [22]: enable minimally invasive intrapericardial therapeutic delivery having an articulated design to provide unlimited but controllable flexibility.

Figure 6. Distal apparatus of the CardioARM

The CardioARM consists of 50 rigid cylindrical links serially connected by three cables, housing flexible working ports through which catheter-based tools for therapy and imaging can be advanced. Two adjacent links can rotate approximately ±10 degrees relative to each other. The current distal apparatus is 10 mm in diameter and 300 mm in length, with 105 DoFs. A novel feature of this mechanism is that all of the links do not have to be individually controlled; this device is sometimes called a "follow-the-leader" mechanism.

- I-Snake [6]: robot with fully articulated joints, allowing the tool to move around obstacles just as a snake can. The joints are powered by micromotors, and the tip is fitted with multiple sensing and imaging mechanisms.
- IREP (Insertable Robotic Effector Platform) [21]: 17-DoF surgical robotic system that can be deployed into body cavity through a Ø15mm skin incision; it consists of two snake-like continuum robots as slave surgical assistants for tissue manipulation, two parallelogram mechanisms for the continuum robots' placement, and one controllable stereo vision module with integrated light source for depth perception and tool tracking.

Continuum robots have also their drawbacks. They have not yet the necessary compliance to exhibit large strains during operations, which would be preferable in surgeries with the minimum discomfort for the patient. Soft robots instead, have the advantage over hard hyper-redundant robots in that they generate little resistance to compressive forces so conforming to unpredictable environments. Therefore, they can carry fragile and soft payloads without causing damage [16].

1.5 Soft robotics: a new challenge

Soft robotics is a bioinspired evolution in robotics: animals are made of soft structures and they use them to adapt themselves in a flexible and compliant way to the environment around them allowing locomotion and exploration of the world.

Drawing inspiration from the natural world, these robots are made of soft, elastic and deformable materials

and they conform to surfaces permitting greater contact area, distributing stress over a larger volume, so reducing the impact force.
Structures like these ones would avoid the risk of accidental and dangerous contacts between machine and patient (e.g. Da Vinci); they are also so compliant due to the materials they are made of (like elastomers), so they can squeeze in very little holes smaller than their nominal dimensions, causing less tissue trauma than rigid instruments, during insertion and navigation through soft tissues and complex organ geometries [17].
Soft robots fall into a class of systems termed 'underactuated' because, unlike hard robots, there is not an actuator for every degree of freedom. The actuators of soft robots are typically integrated and distributed throughout the structure preventing the use of many traditional hard actuators such as electric motors [23] which implies a mechanical self-stabilization and lighter bodies.

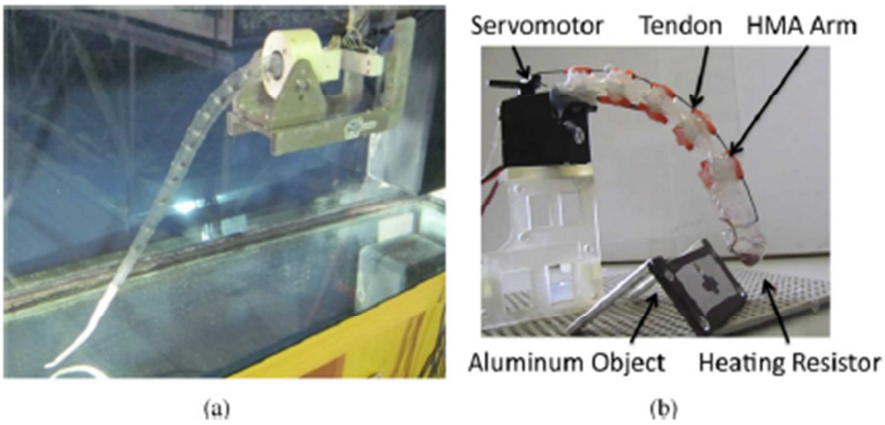

Figure 7. Recent development of soft robotics research [24]. (a) A prototype of octopus robot that makes use of flexible skin driven by SMA actuators (developed at The BioRobotics Institute, Scuola Superiore Sant'Anna). (b) A prototype of soft robot manipulator made of Hot Melt Adhesive (developed at Bio-Inspired Robotics Lab, ETH Zurich).

In the development of soft robots significant challenges remain the choice of the materials, the electromechanical design, fabrication and sensing.
Soft robots' structure is a continuum, they theoretically have infinite DoFs, but exact measurements are difficult because the number of sensors and actuators is finite and because conventional technologies as high-resolution encoders cannot be easily transferred from their hard counterparts; furthermore the environment applies loads to the soft structure either through distributed loading (e.g. gravity) or by contact causing continuous deformation. Models that accurately describe the large-deflection dynamics of soft robots are generally too expensive computationally to be useful for real-time control [16].
Designing the manipulator, is important to find a trade-off between providing sufficient dexterity and maximising load capacity because a soft robot that performs optimally for an entire range of tasks is difficult; furthermore, their tasks require a certain amount of force, while flexibility and softness are usually accompanied by limited force capability.

1.6 The STIFF-FLOP project

Thus was born the idea of the STIFF FLOP, a modular soft variable stiffness manipulator for minimal access surgery. It takes inspiration from biological manipulation and actuation, principles found in the octopus that can turn its links from a completely soft state into a state of powerful and stiff articulation.
Current devices are generally externally actuated and have an underactuated structure with a compliant backbone which results in low stiffness at the end effector not providing the necessary support.
STIFF-FLOP instead combines the possibility of a variable stiffness to the ability to squeeze through narrow gaps and openings (12 mm diameter) due to his inherent compliance, hyper-redundancy for improved reachability in an obstacle-cluttered environment like our body and increased adaptability and stability in a possibly unpredictable environment, taking advantage of the best of soft and rigid robotics.
The manipulator will be composed of multiple identical modules, everyone capable of independent bending in various directions, elongation and stiffening [25].

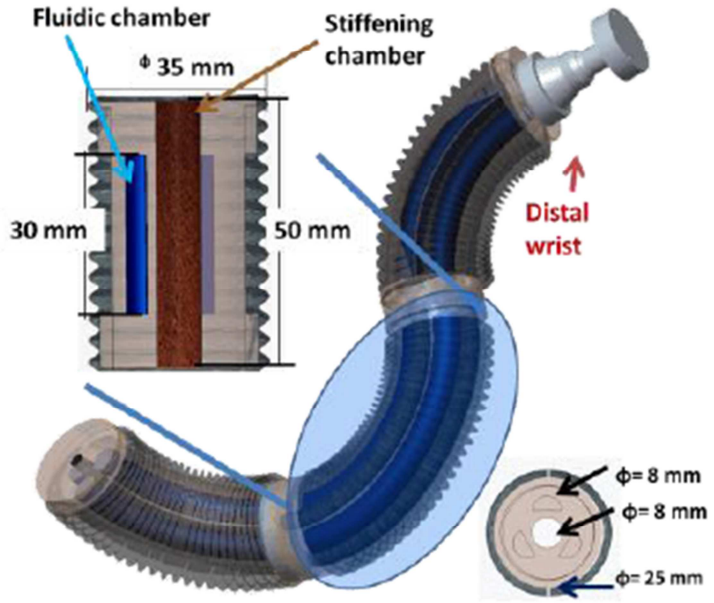

Figure 8. Architecture of STIFF-FLOP

As shown in Figure 8, every module is composed of a silicone cylinder. Inside this cylinder there are three equally spaced semi-cylindrical chambers in radial arrangement (the fluidic actuators) and another one centrally placed (for the stiffening mechanism). Several analysis methods have been used to investigate the best geometries and in conclusion the best one is a trade-off between the thickness of the separation wall between the chambers and their diameter [26].
The inflation of one of the fluidic chamber causes a bending coupled with an expansion in the radial direction: in fact, a drawback of using soft materials actuated by pressurized fluids is their low mechanical efficiency. In order to constrain the lateral deformation a crimped braided sheath has been introduced around the cylinder, considering that the elastomeric materials are isotropic: the braided sheath can provide a radial constraint and at the same time follow the robot movements. When one or two chambers are inflated, the robot starts to bend with a bending angle and radius depending on the input pressure and on the utilized chamber: the angle is bigger with only an actuated chamber, but with two actuated chambers the bending radius is emphasized [27]. Elongation is then obtained by activating the three chambers simultaneously. The typical maximum elongation for every chamber is around 100%, so the maximum reached dimension is 60 mm.
The central chamber is fabricated filling coffee powder in a latex membrane, and stiffening is produced using a vacuum pump, and depending on the level to which it is adjusted, a more or less rigid system is

obtained. The stiffening modulation plays a key role due to the need of having a compliant but also rigid robot during manipulation.

CHAPTER 2: SENSING FOR MINIMALLY INVSIVE SURGERY

2.1 State of the Art

As demonstrated in [28], sensing feedback enhances the performances in MIS, while its absence could increase the tissue trauma damage, especially when the involved structures are so sensitive that traumas can lead to severe implications. In order to restore the surgeon's perceptual capability in MIS, methods of sensing [7] have been applied with attempts to develop instruments that can be used to detect forces and generate feedbacks to the surgeon.

Sensing elements also significantly improve the performance of robotic surgical systems: with sensing, robots are expected to intelligently perform in unstructured and changing surroundings then to work more autonomously and to be more responsive to unexpected contacts by detecting contact forces during activities such as manipulation. Also, the ability to perceive their own state is important in surgical robots and affects the performance of the operation.

To achieve this goal, robots need an interface that can provide information about the forces and positions at all points of contact between them and the objects they are interacting with [29].

Then, sensing elements must be integrated with the instruments. Size and complexity of such elements depend on the degrees of freedom required for the measurement. In traditional medical instrumentation there are four locations where they could be placed:

1. Near or at the actuation mechanism driving a joint by monitoring stress of the mechanical linkages or responses of the actuators.
2. On the instrument shaft outside the patient's body.
3. On the instrument shaft inside the patient's body.
4. At the instruments tip.

The choice must take into account the space limitations in MIS, the friction and reaction forces created at the instrument insertion port and various other errors in the measurement.

Another important issue is the sterilizability, and the most common method is the autoclave which employs saturated steam to heat the equipment up to 121 C at 103 kPa above; for this reason the intensive heat, pressure, and humidity can potentially destroy sensors and electronics so sometimes, chemical sterilization protocols using chemical agents are used.

Magnet resonant imaging (MRI) compatibility is often an important requirement for surgical robots and for the sensor to be integrated onboard as well.

Sensors can be classified according to different criteria, as the type of measurand (acoustic, biological, chemical, electrical, etc.) or the nature of the output signal (digital or analog); in choosing a sensor for a given application, it is also evident that the physical principles on which they operate is an important factor as a sensor using a particular principle may perform much better than another one using a different principle in given operating conditions.

In Table 1 various examples of the physical principles exploited in measurement sensors are reported.

Physical Principle	**Typical application**	**Measurand**	**Output**
Resistive: the variation of the electric resistance of the sensing element varies depending on the measurand	Thermistor, potentiometer	Temperature, displacement, force pressure, flow, humidity	Resistance
Capacitive: two conductive plates with a dielectric material sandwiched between them. Their capacitance depends on the	Rotary plate capacitor sensor, differential capacitor	Displacement, force, angular position, torque	Capacitance

measurand			
Inductive: the sensing element inductance depends on the measurand	LVDT, self-inductance transformer	Displacement, thickness, conductivity	Inductance
Reluctive: the variation in the reluctance path between two or more coils depends on the measurand	Rotary variable differential transformer	Angular rotation, position, torque	Reluctance, Voltage
Piezoresistive effect: resistance of the sensing element depends on the strain	Strain gauge: typically long winding snakelike structures; when deformed, the cross-section of the strain gauge decreases while its length increases	Stress, strain, pressure, force	Resistance
Total internal reflection: in an optical fibre, the light travels through the core by constantly reflecting from the cladding, so it is used as a medium to carry force information from a sensing region to optoelectronic equipment.	Fabry perot interferometer, distributed Bragg reflector	Strain, shape, temperature, force, liquid level	Voltage or current
Electromagnetic: based on the Faraday's law: in any circuit capturing a magnetic flux, whenever the flux changes an electromotive force is induced	Flowmeter, linear velocity sensor	Linear velocity, flow, angular speed, torque, magnetic field	Voltage
Hall effect: if the sensing element, carrying current, is put in a magnetic field, a difference in electric potential among its sides is generated	Gaussmeter, Wattmeter	Magnetic field, displacement, power	Voltage
Magnetoresistive effect: resistance of the sensing element depends on the strain	Magnetoresistor	Magnetic field, linear and angular displacement, proximity, position	Resistance
Piezoelectric effect: subjecting the sensing element to stress, there is a generation of electric charge	Vibration cables, force sensors, piezoelectric microphone, temperature sensor	Vibration, force, ultrasonic waves, temperature	Voltage or charge
Pyroelectric effect: the	Pyroelectric sensor	Change in temperature	Voltage

sensing element generates an electric charge in response to heat flow			
Photoresistive: the electric resistance of the sensing element is caused by the incidence of optical radiation	Photoresistor, photodiode, phototransistor, photofet	Light, position, motion, force	Resistance

Table 1 [30]: Examples of physical principles of sensing devices.

2.2 Sensing for continuous and soft robots

Particular attention should be paid to continuum-like and soft robots: these robots can bend (and often extend/contract, twist) at any point along their structure. This provides them with capabilities beyond the scope of their rigid-link counterparts [31], allowing them to perform whole arm manipulation. On the other hand they introduce new challenges to present a sufficiently compliant and controlled interface to avoid breakage of the manipulated objects.

Continuum-like robots' models necessarily differ significantly from those of conventional rigid-link robots, where kinematic variables (joint angles/displacements) completely determine the shape of the robot: a common used method in rigid robotics for the definition of the kinematic model of a robot manipulator is the Denavit–Hartenberg convention (D–H) through which it is possible to describe the positions of links and joints unambiguously.

It is important to plan trajectories which simultaneously permit to avoid obstacles and grasp objects. The existence of practical, real-time, sensor-based motion planning algorithms will be necessary because user interfaces for continuum robots is a relatively neglected and poorly understood topic. The movements of continuum elements are often counterintuitive to human operators, much more than for rigid-link robots, leading to confusion or limited exploitation of all the possible motions of the robot.

In surgery, when applications become more challenging, the desire for more accurate models is desired [16] as it could enable operation in the proximity of humans [32] but sensing and controlling the shape and motion of continuum and soft robots is more complicated due to their structural flexibility. These are problems that must be addressed rigorously, equipping robots with the correct proprioceptive and exteroceptive sensors: intrinsic or proprioceptive sensors use global measurements from which indirect information can be extracted [33] as contact and bending information. These sensors include force/strain sensors, optical sensors and joint torque sensing. They are usually placed within the mechanical structure of the system; extrinsic or exteroceptive sensors can sense contact location and, in some cases, contact pressures and shear stresses, monitoring the external environment, mounted at or near the contact interface and deal with the data from localized regions [34].

The same considerations of continuum robots can be done for the soft ones, but care should be taken about their being inherently compliant, and therefore the need of non-rigid sensors.

Furthermore here external loads and gravity cause a deviation (as shown in Figure 9) from constant curvature that become a much more significant factor when result from environmental contacts.

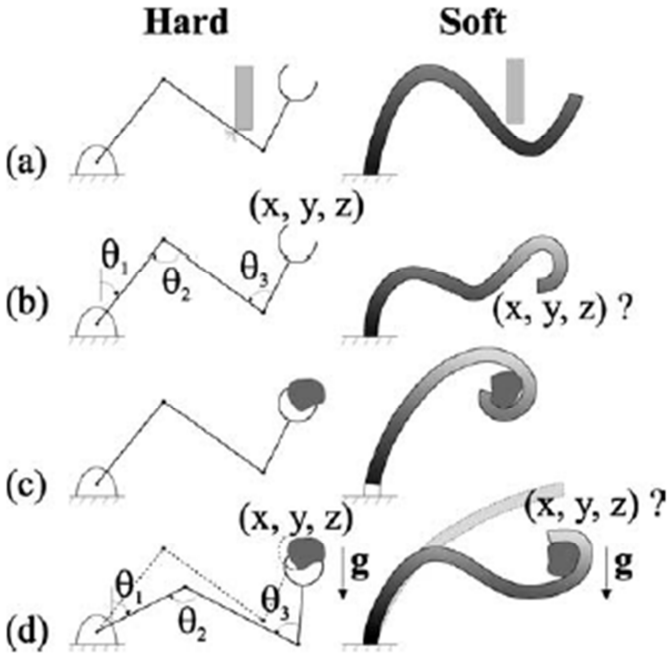

Figure 9. Comparison between hard and soft robots: a) dexterity, b) position sensing, c) manipulation and d) loading

As already mentioned use of continuum and soft robots needs different models of robot shape and motion and the existence of practical, real-time, sensor-based motion planning algorithms is necessary.
A simplified approach approximates the soft robots with a "piecewise constant curvature" [35] as composed of finite circular arcs, each with a set of parameters which can be converted in position and orientation information, from the configuration space to the task space of the robot with a purely kinematic mapping (Figure 10).

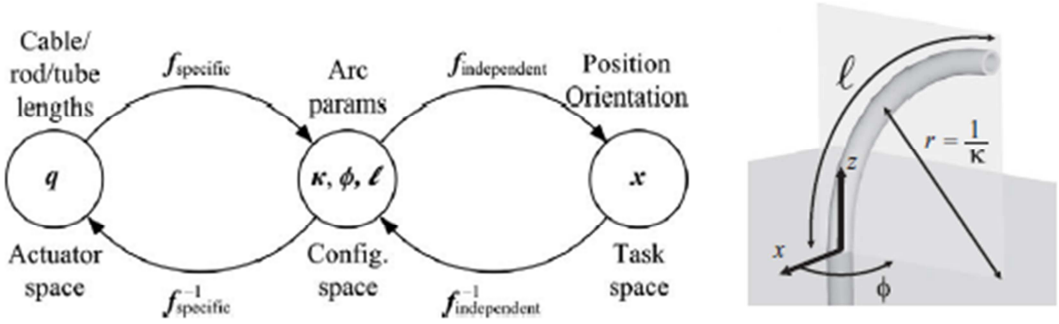

Figure 10. The three spaces and mappings defining the kinematics of constant-curvature robots and the arc parameters are shown.

The arc parameters are a triplet of curvature *k*, the angle of the plane containing the arc *Ø*, and the arc length *l*. The kinematic mapping from actuator space *q* to the arc parameters is robot specific. If we wanted to calculate the arc parameters we have to know the joint variables q = [l_1, l_2, l_3], indicating the length of three sensors (evaluating the length of the three pneumatic chambers).

$$l(q) = (l_1 + l_2 + l_3)/3 \qquad (1)$$

$$\emptyset(q) = tan^{-1}\left(\frac{\sqrt{3}(l_2 + l_3 - 2l_1)}{3(l_2 - l_3)}\right) \qquad (2)$$

$$k(q) = \frac{2\sqrt{{l_1}^2 + {l_2}^2 + {l_3}^2 - l_1 l_2 - l_1 l_3 - l_2 l_3}}{d(l_1 + l_2 + l_{3)}} \qquad (3)$$

Where d is the distance from the centre of a section of the robot to the centre of the sensor (the same for every sensor).
This can be also applied to multi-section robots, considering independently each section.
For the aforementioned reasons we propose to use three length sensors inside every silicone module of the STIFF-FLOP robot, equally spaced from the three pneumatic chambers, as shown in Figure 11. Measuring the length of the three chambers it is possible to calculate the arc parameters.

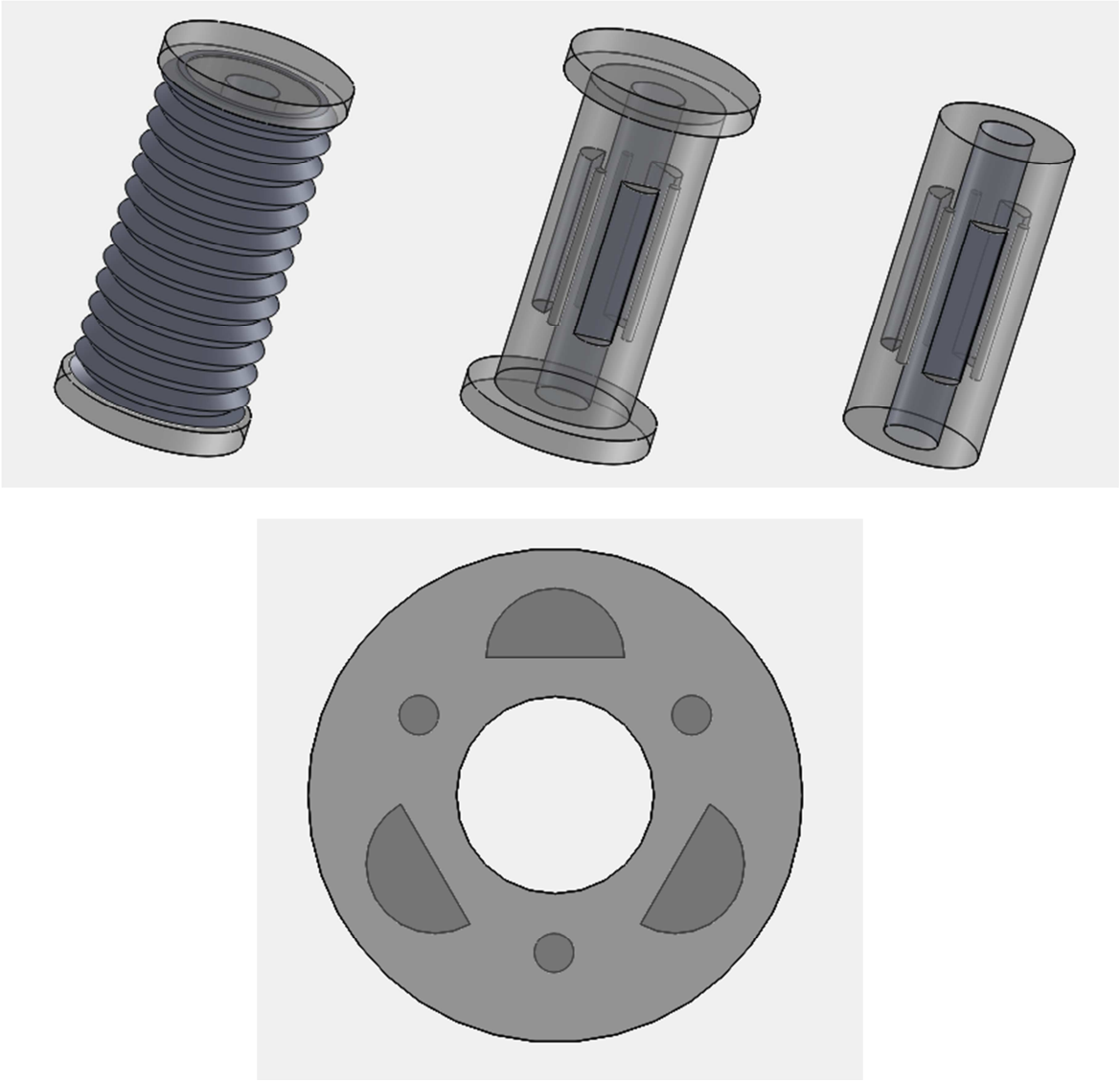

Figure 11. Integration of the soft sensor inside the STIFF-FLOP robot

Seems obvious that these sensors have requirements as a result of their application. They should be soft and stretchable to not interfere with the module elongation and bending; sense strain and not pressure

inside the chamber; furthermore they should be non-toxic and biocompatible, small and functional when stretched.

2.3 Stretchable Sensors

As aforementioned, with the advent of the direct physical interaction between robots and humans, various types of contacts can occur during whole-body close interaction. In particular in the case of soft or highly compliant robots the contact region can be extended and is not limited to the end effectors as for rigid robots [8]. Sensing forces at the operational point might not be enough when the workspace of the surgical robot is surrounded by delicate tissues and vital organs. Ideally, the entire robotic structure should safely move with contact and bend detection along its entire body [36]. For these reasons the use of sensors elastically soft which remain functional when stretched to several times their natural length becomes necessary. In contrast to existing thin-film solutions that are flexible but not stretchable, this generation of sensors must be able to conform the changes in shape and in rigidity without interfering with the natural mechanics of the robot [37]. Also, for the best integration, sensor element itself should be small. Different approaches for stretchable sensors have been explored over the years, as shown in Table 2, but in spite of their flexibility these sensing technologies are not truly stretchable, because they often use solutions in which rigid sensing elements are integrated in a supporting elastic substrate, following and limiting its deformation, and so they cannot remain functional at large strains.

Application	Sensing strategy	Material	Stretchability	Stiffness	Bandwidth	Sensitivity range	Repeatability and accuracy	Hysteresis	Availability	Cost	Temperature dependency	Integration strategy	MRI compatible	Ref
Measuring the bending curvature	Optical sensor: light intensity modulation	Plastic resin EcoFle	Yes	Medium		2-15 mm sensitivity (distance from the reflected surface)			Research prototype	Low	No	Integrated but there are drawbacks due to the fibre dimension	Yes	[38]
Force Sensor for Cardiac Catheterization Procedures	Optical sensor: light intensity modulation	Optical fibres made of acrylic material		Medium	Up to 3Hz	Sensitivity range:0–0.85 N Resolution < 1g	Good accuracy	Small	Prototype	Low	Not	Fully integrated	Yes	[39]
Soft Sensor Flesh for whole body tactile sensor system	3-axis force/torque sensor	Soft urethane foam cube.	Yes			Senses applied force from 0 to about 1.4 kgf	Not so high accuracy	Little due to the urethane	Prototype	Generally low, depending on the fabrication method	Not high heat conductivity	Robot covered with soft material, with sensors embedded inside the exterior and others moulded and placed in its middle depth.		[8]
Active catheters	Piezoresisitive	Nitinol: Shape memory alloy (SMA)	Yes	Depends on the geometry and dimensions. In general is little stiff		Sense 150–450 µm elongation	Good accuracy	Not	Prototype		Yes	Mounted on the catheter, designed as a winding structure		[40]

Electronic skin applications	Capacitive sensor	Gold thin films embedded in silicone rubber PDMS	Yes, up to twice its length			Sensitivity range: up to 160 kPa	Repeatability	No	Prototype			Easily integrated due to its dimension		[41]
Skin-like tactile sensor	Piezoresisitive	Silicone-Carbon Black layer (conductive) with an Au thin film deposited	Up to 14%.			Testing range 0 N/mm2-0.16 N/mm2	High repeatability	Low	Prototype			Not studied		[42]
Ground Reaction Force sensor in the sole of a humanoid robot foot	Piezoresisitive	Polyimide and Polydimethylsiloxane used as substrate and thin metal strain gauges	Yes	No		Normal loads up to 4N, low sensitivity	Inaccurate for small loads		Prototype	Low		Easily integrated due to its dimension		[4]
Normal and Shear Force Measurement for robot hands	Capacitive sensor	Two thick Polydimethylsiloxane (PDMS) layers with embedded electrodes, an air gap, and a pillar structure.	Yes			2.5-3%/mN		Negligible for small deformation				Easy integration due to its dimension		[43]
Element for tactile sensor skin	Capacitive sensor	Two layers of urethane foam insulators sandwiched between three stretchable conductive sheets	Yes						Prototype			Integrated in the robot skin		[44]
Measurement of contacting force for robot-joints	Resistive based	Two silicone rubber channels filled with electro conductive liquid.	Yes	No				No	Prototype			Mounted in the robot joint		[45]

Touch Sensor for electronic skin	Piezoresisitive	Layers of monolayer-capped nanoparticles (MCNPs)on flexible substrates	Yes	No		Senses from 0.2 mN to 0.1 N	Good accuracy		Prototype		Not reported			[46]
Conformable TactArray Pressure Sensor		Not specified: soft conductive cloth	Yes			Senses from 0 to 1.400 kPa			Commercial device					[47]
Strain Sensing Fabric	Piezoresisitive	Conductive mixture directly spread over the fabric	Yes		0-10 MHz	Testing range from 0 to 240 µm			Prototype			Integrated in a glove for gesture monitoring		[48]
Artificial skin	Piezoresisitive	Copper wires around an elastic nylon line placed on a Polydimethylsiloxane (PDMS) substrate	Yes			Senses from 0 to 450 kPa			Prototype					[49]
Artificial skin	Capacitive sensor	Closed-cell silicone foams			0-80 Hz	Senses from 0.02 to 100 N		No	Prototype	Low		Integrated in the artificial skin		[50]
Exoskeletal Force-Sensing	Optical sensor: fiber Bragg grating		Yes			Senses force changes of less than 0.02 N	High accuracy	No	Prototype	Low	Yes	Embedded sensors in the exoskeleton		[51]
Shear stress sensor for tactile sensing	Piezoresistive	Piezoresistive cantilevers embedded in an elastic material	Yes			Senses shear from range of −5.0 to 5.0 kPa.	High accuracy	No	Prototype				No	[52]

Table 2: Overview of flexible sensors

2.4 Liquid-embedded elastomers

For the aforementioned reasons a novel approach uses a silicone rubber film with conductive liquid-filled microchannels. Applying pressure or stretching to the surface of the elastomer deforms the geometry of the underlying microchannels changing their length L, width W, and thickness T, so the electrical resistance:

$$\Delta R = |R - R'| = \rho \left| \frac{LW}{T} - \frac{L'W'}{T'} \right| \qquad (4)$$

where ρ the liquid resistivity and ΔR the change in resistance.
The advantage of elastomers is their hyperelasticity [53], so mechanical durability and stretches as great as 1000%. Furthermore liquid conductors eliminate the need for rigid electronics and preserve the natural elasticity of the embedded elastomer.
When the material experiences strain in the axial direction of the channels [54], the overall channel length increases and the cross-sectional areas of the channels decrease, which causes an increase in the overall resistance of the channel, instead pressing the surface of the elastomer skin decreases the cross-sectional area of the microchannels and increases their electrical resistance.

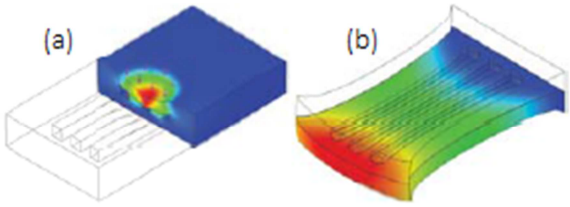

Figure 12: Hyperelastic sensor design concepts. (a) Pressure sensing. (b) Strain sensing

As demonstrated in previous works the same principle can be also used to measure curvature and bending; in [37], Majidi et al. developed a sensor composed of two rectangular elastomer plates attached at opposite edges and at the centre by a parallel strut, where a microchannel filled with conductive liquid is embedded above the strut. Referring to Figure 13, as the plates bend, compressive force induced in the strut exerts a pressure on the embedded channel, which consequently deforms; bending curvature is inferred from the relative change in electrical resistance of the embedded microchannel.

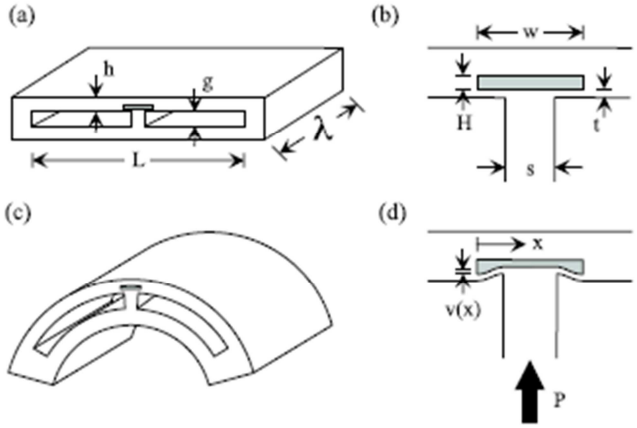

Figure 13: (a) The curvature sensor composed of two thin films separated by a gap and bonded along their two ends as well as along their midline by a strut. (b) One of the films contains a microchannel filled with liquid. (c) Bending

induces a compressive force that (d) causes the embedded channel to collapse.

In order to determine the sign of bending curvature, two curvature sensors could be placed on top of each other: the sensor embedded inside the inner film will register a smaller change in electrical resistance. Therefore, the sign of bending curvature is determined by identifying the sensor with the smaller measured ΔR.

Kramer et al. introduced a different combined strain and bending sensor which can be used to measure both of the signals, with a combination of different geometries, presenting a serpentine channel and a perpendicular strut [55]. This sensor was mounted on a finger with the sensing element positioned on top of the knuckle. When the finger bends, the elastomer is stretched and subjected to pressure on the sensing element, thus leading to a change in the electrical resistance of the channel.

Different geometries have been explored for various application, for example perpendicular conductive serpentine-like channels within an elastomeric matrix forming a network that is used like a keypad [56], registering the location, intensity and duration of applied pressure, as shown in Figure 14.

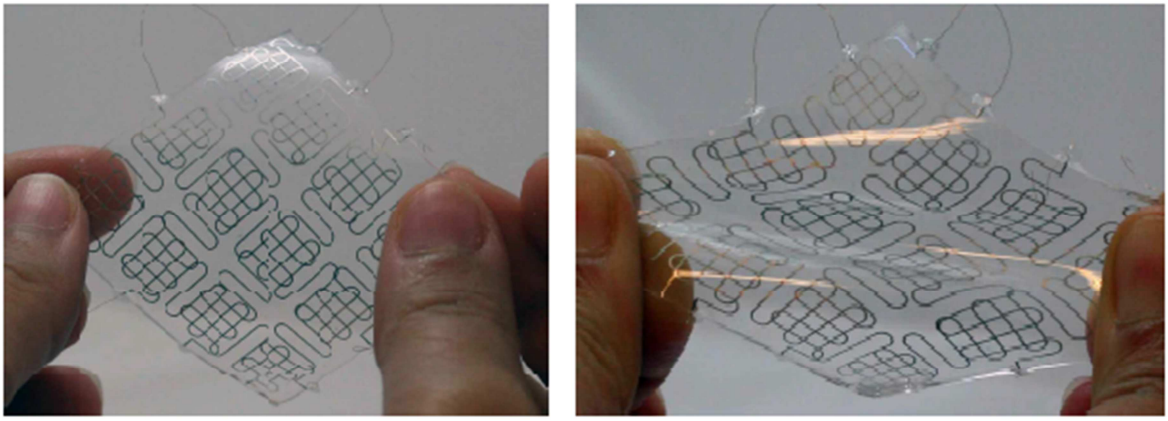

Figure 14. The elastomeric keypad at its minimum energy configuration and when stretched.

Other studies include three sensor layers as shown in Figure 15: using the combination of the signals from the sensors, the device is able to detect and distinguish three different stimuli: x-axis strain, y-axis strain, and z-axis pressure [54]. In this work the sensor signals for strain sensing were approximately linear, so simultaneous strain measurement of both axes was achieved by determining a calibration matrix, while pressure response was found to be non-linear.

A different physical principle has been studied as a soft capacitive sensor, where a sheet of elastomer is embedded with fluidic capacitors [57] (Figure 16). When the elastomer changes is shape due to pressure or stretching, the electrodes of the capacitors move, leading to a change in capacitance. The magnitude and direction of the deformation is obtained comparing the change in capacitance of multiple embedded capacitors.

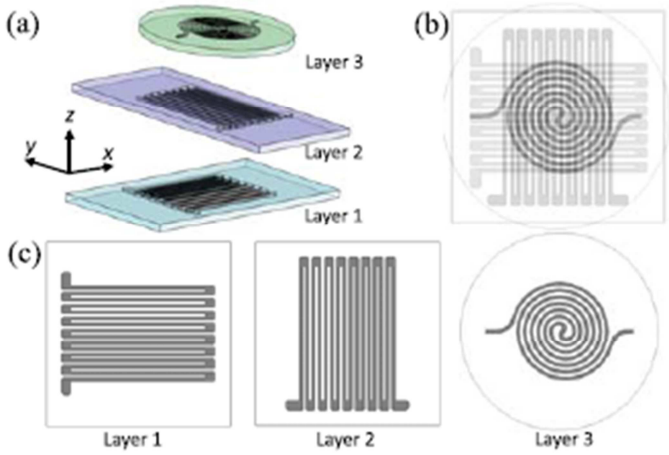

Figure 15: Design of the three sensor layers with embedded microchannels. (a) Exploded view. (b) Assembled view. (c) Each sensor layer design

Figure 16: The soft-matter shear sensor.

CHAPTER 3: PROPOSED SOLUTION

Previous aforementioned works in soft sensors have used a particular type of conductive liquid material, eutectic gallium-indium (eGaIn) [58] which is finding increasing applications in soft wearable robots, flexible sensors and stretchable electronics. eGaIn is an alloy of gallium and indium maintaining a liquid state at room temperature and has a resistivity $\rho = 29.4 \times 10^{-8}\ \Omega\ m^{-1}$. Due to its high surface tension and high electrical conductance, eGaIn is an ideal conductor for a soft sensor. The high surface energy of eGaIn allows a channel to be filled and remain intact even if the channel inlet and outlet are exposed, so the basic principle of the manufacture was to create empty structures of elastic material to be filled with eGaIn and to wire it to a measurement system.
The drawback in using eGaIn is that, even if is non-toxic, this alloy is still not biocompatible: biocompatibility is the ability of a biomaterial to perform its desired function with respect to a medical therapy, without eliciting any undesirable local or systemic effects [59]; the development of alternate conductive fluids is therefore needed for medical applications [60].
For this reason, we introduce a small, low-cost, soft and stretchable sensor composed of a silicone rubber, integrating a conductive liquid channel filled with biocompatible Sodium Chloride (NaCl) solution.

3.1 System geometry

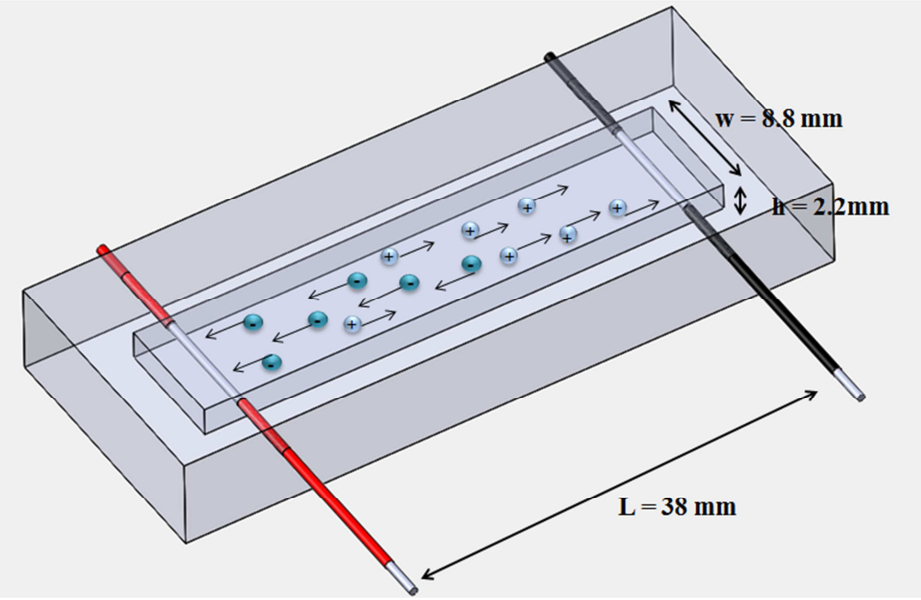

Figure 17. View of the silicone sensor: when a voltage difference is applied between the electrodes inside the solution, the Na^+ and Cl^- ions are attracted respectively to the negative anode and the positive cathode. As charge carrier, their movement inside the solution generates a current.

When strain is applied in the axial direction of the channel, the length increases and the cross-sectional area of the channels decreases, thus causing an increase in the resistance between the electrodes. For the chosen geometry, the theoretical relationship between the resistance change ΔR and strain can be found as follows [54]:

$$\Delta R = R - R_0 = \rho \frac{L + \Delta L}{(w + \Delta w)(h + \Delta h)} - \rho \frac{L}{wh}, \quad (5)$$

where ΔR is the difference between the resistances of the channel when stretched by ΔL and not stretched, and ρ is the resistivity of the solution.
Poisson's ratio v is the ratio of transverse contraction to longitudinal extension strain in the direction of the applied load. For the overall volume constancy, when the channel with diameter (or width, or thickness) d and length L is subject to stretch so that its length will change by ΔL then its diameter d will change by:

$$\Delta d = -d\left(1 - \left(1 + \frac{\Delta L}{L}\right)^{-v}\right) \qquad (6)$$

Since $\varepsilon = \frac{\Delta L}{L}$ and $v = 0.5$ for an elastomer material, it is possible to simplify the above equation as follows:

$$\frac{\Delta R}{R_0} = \varepsilon(2 + \varepsilon) \qquad (7)$$

That means that the resistance variations are quadratic with the strain, as shown in Figure 18.

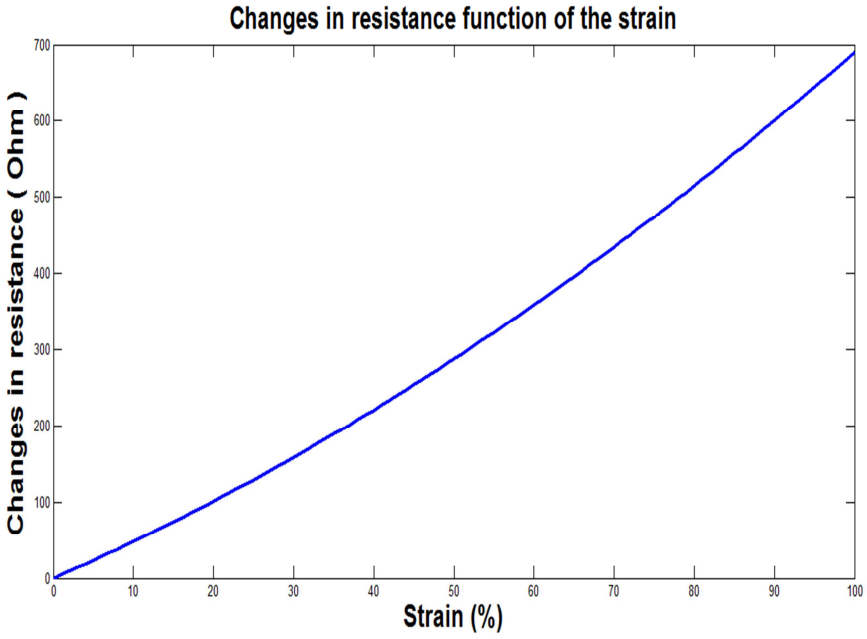

Figure 18. Theoretical behaviour of the sensor changes in resistance function of the strain.

3.2 Conductive liquid

Liquid conductors, eliminating the need for rigid electronics and preserving the natural elasticity of the sensor, are good candidates for a soft sensor; furthermore, NaCl solution fulfills the need for a biocompatible liquid. Compared to eGaIn, NaCl solution has different physical properties, and so a different behaviour when used in liquid filled soft sensors. In particular, the surface tension of eGain is 624 mN/m

while 1 mole of NaCl has a surface tension of 1.64 mN/m, which creates more difficulties when filling a microchannel.

Electrolytic solutions as NaCl are defined as aqueous solutions in which the Na^+ and Cl^- ions are surrounded by the polar water molecules and so become free to move, allowing electric current to be conducted: when a voltage is applied across electrodes inside the electrolytic solution, electricity conduction takes place because these ions move according to their positive or negative charge.

The choice of the dilution, according to the resistivity that we want is an important parameter; we should also take care of having a perfect dissolution.

The use of an ionic solution introduces constraints in the design of the associated electrical circuit since the electrolysis of the solution and polarization of the electrodes must be avoided: when current starts flowing, the ions start concentrating at the interface of the conductor up to create a barrier to the current flow and it will create an electric double layer, and then an overvoltage which results in a variation of the measured voltage. Polarization of the electrodes under a direct current (DC) causes the formation of this double layer at the electrodes and hence the sensor would in part behave like a capacitor.

For this reason we used a 500mV AC voltage at 4kHz [61] for its excitation (as it is a passive sensor). This frequency was chosen because signals at high frequency are less dangerous since they excite less cells: the most dangerous signals are those with a frequency range between 10 and 1000 Hz [62].

Sodium chloride is a strong electrolyte as it is dissociated in water up to relatively high concentrations (37.0 g/100g of water at 25°C) [63].

Taking inspiration from previous works with NaCl solutions [61], 1g of salt was dissolved in 10 ml of water; resistivity of the solution is then calculated from a resistivity table as shown in Figure 19 [64].

Considering a temperature of 25° C and a ppm (parts per million) of 100000, it was found that ρ=0,075 Ω*m.

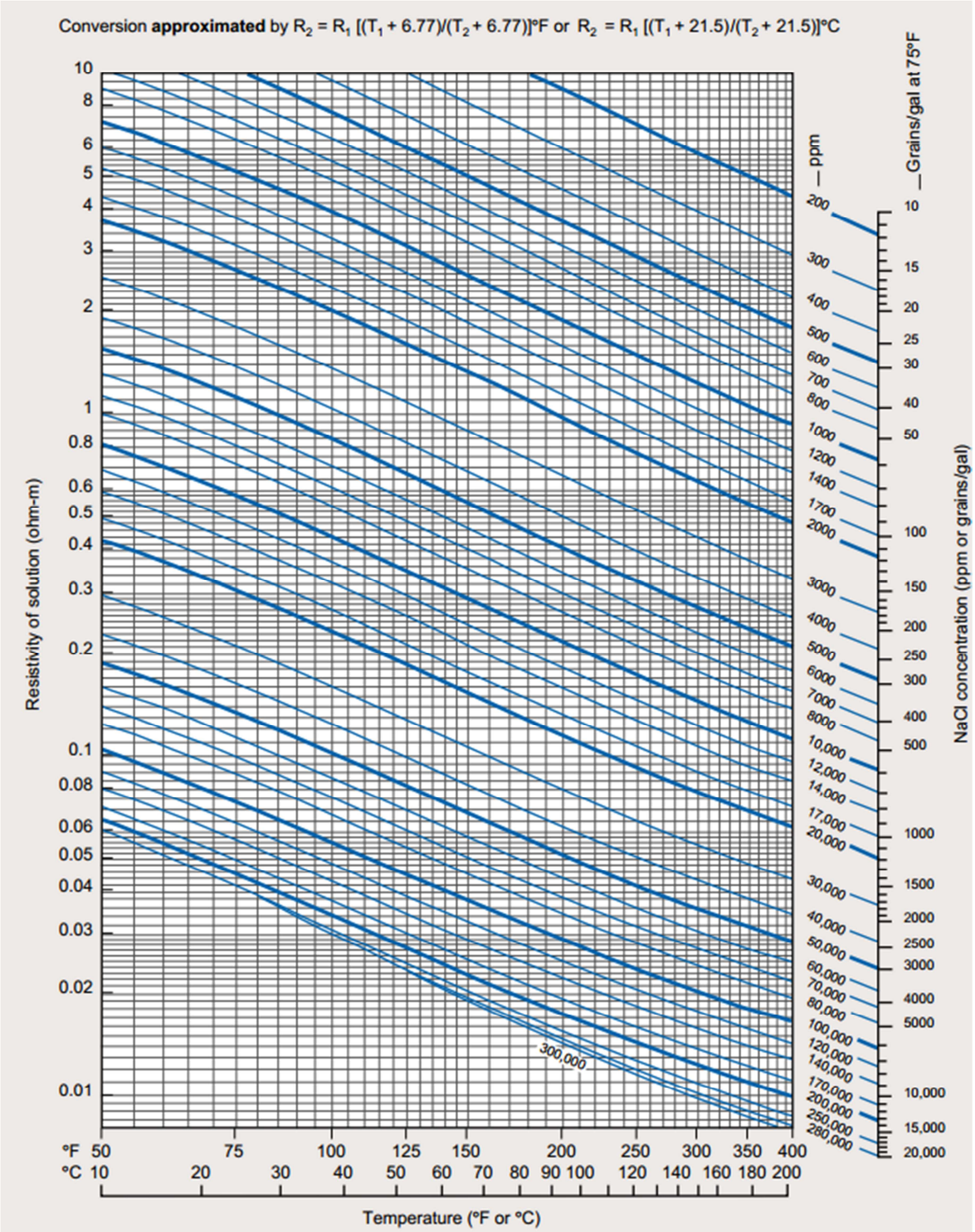

Figure 19. Resistivity table for a NaCl solution.

3.3 Silicone rubber

Ecoflex rubbers [65] are platinum-catalyzed silicones that are versatile and easy to use. They are mixed 1A:1B by weight or volume and cured at room temperature with negligible shrinkage. Their low viscosity enables easy mixing but this causes the formation of entrapped air, so vacuum degassing is recommended

to minimize air bubbles in cured rubber. Vacuum degassing chambers are used for making bubble free castings: the lid is made from shatter resistant acrylic and features a rubber gasket that creates a positive, air tight seal for maximum vacuum. After inserting the mixture inside the chamber, we place the lid on the pressure chamber and tighten the wing nuts, attaching then an air supply hose.
After some minutes the air pressure valve can be released and the bubble-free mixture is casted into the mold. Finally the rubber is cured at room temperature or in the oven at 50-60 °C for 30 minutes before demolding.
After curing, the elastomer is removed from the molds (Figure 20): the rubber is water white translucent, soft, strong and stretchable many times its original size without tearing, rebounding to its original form without distortion. These rubbers are available in different hardness and we choose the softer one (EcoFlex 0030 SmoothOn).

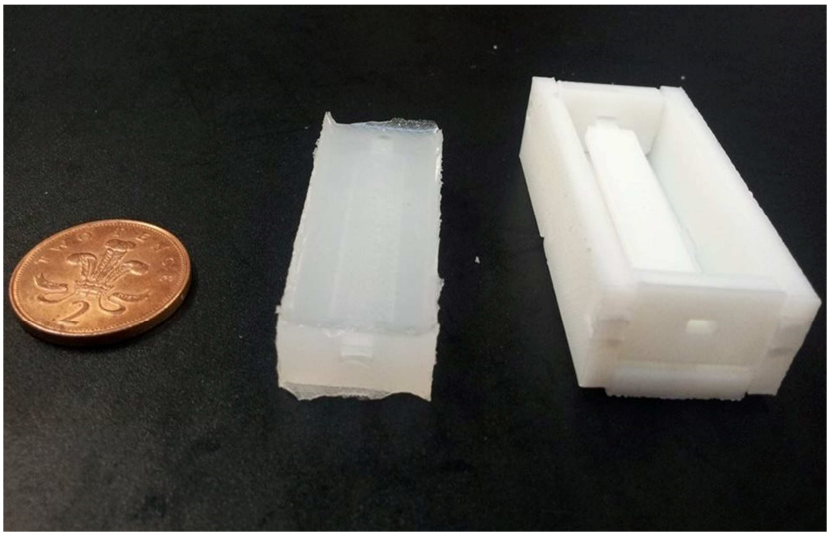

Figure 20. View of the mold and the cured silicone with an embedded channel.

The advantage of using silicone rubber is its mechanical durability and high flexibility, non-toxicity, chemical stability and low cost [65]; silicone rubber sensor does not limit the overall deformation of the host, does not interfere whit its mechanics and in our case the STIFF-FLOP robot and the sensor are made of the same material.
For manufacturing reasons and for the first feasibility studies, we chose the dimensions of the channel as length L = 38 height h = 2.2 and width w = 8.8 mm, for having the necessary channel size to eliminate the bubbles obstructing the current path. In fact, the adhesion force between the saline solution and the silicone is very small and sometimes a small air bubble remains stick to the channel edges; if the channel was too thin, one air bubble could obstruct it.

3.4 Fabrication process

Several prototypes were developed to evaluate the best geometry and a way to connect the electrodes inside the silicon for obtaining a stable structure.
The molds are prepared using a 3D printer which takes virtual blueprints from computer aided design (CAD) and makes a three-dimensional solid object, as shown in Figure 21: SolidWorks is a program being developed by Dassault Systèmes SolidWorks Corp that allows users to develop digital solid models in a simulated environment for both design and analysis.

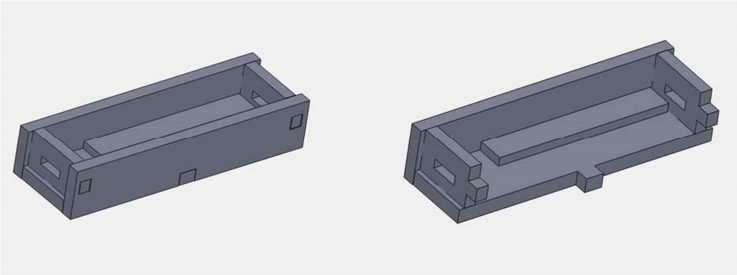

Figure 21. View of the CAD model of the mold.

The silicone rubber is casted inside the molds and after approximately 4 hours at room temperature, the elastomer is cured and removed.
Next, the electrodes are inserted into the ends of the channel, which is closed with silicone rubber; a syringe is used to fill the embedded channel with NaCl solution while another one is used at the same time to capture and remove the air inside the tube. Then, uncured rubber is casted for sealing all the holes and preventing the formation of air bubbles.

3.5 Acquisition system

The sensor has been then experimentally characterized both under tensile and compression stresses. The experimental setup (Figure 22), is composed of a linear stage using a HIWIN linear motor, a multimeter, a laptop and a National Instrument data acquisition (NI DAQ) board.

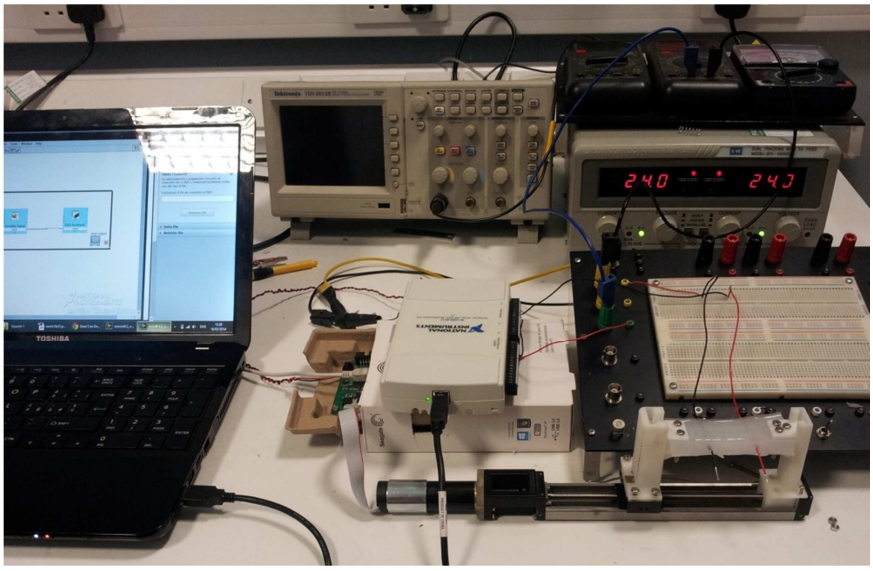

Figure 22. Experimental setup for measuring applied strain and electrical resistance for the sensor prototype. From the right: the laptop, the NI DAQ board, the electrical circuit, the multimeter and the prototype.

The HIWIN stage is used for performing accurate stretching and compression tests. Two rigid 3D printed clamps are fixed around the edges of the sensor and the motor: one is mounted on its fixed part, and the other one on the moving block in which is integrated the ball screw for the linear advance.
These parts have a mobile shelf and screws to fix the silicone rubber; the design was made in Solidworks, taking care of all the device specifications on the motor datasheet.
Tensile tests were performed by imposing quasi static displacements from 0 to 35 mm with a step of 1 mm.

In the first measurement a failure of the silicone has been noticed, due to a fabrication mistake: as shown in Figure 23, the rigid clamps created some compression points in the dead zone of the sensor, holding it with screws. For fabrication reasons, the right side of the prototype was casted afterwards the left part was cured. As a result, an area of stress concentration between the two interfaces was created and to solve the problem in the other tests, the silicone rubber was subsequently casted in one single time.

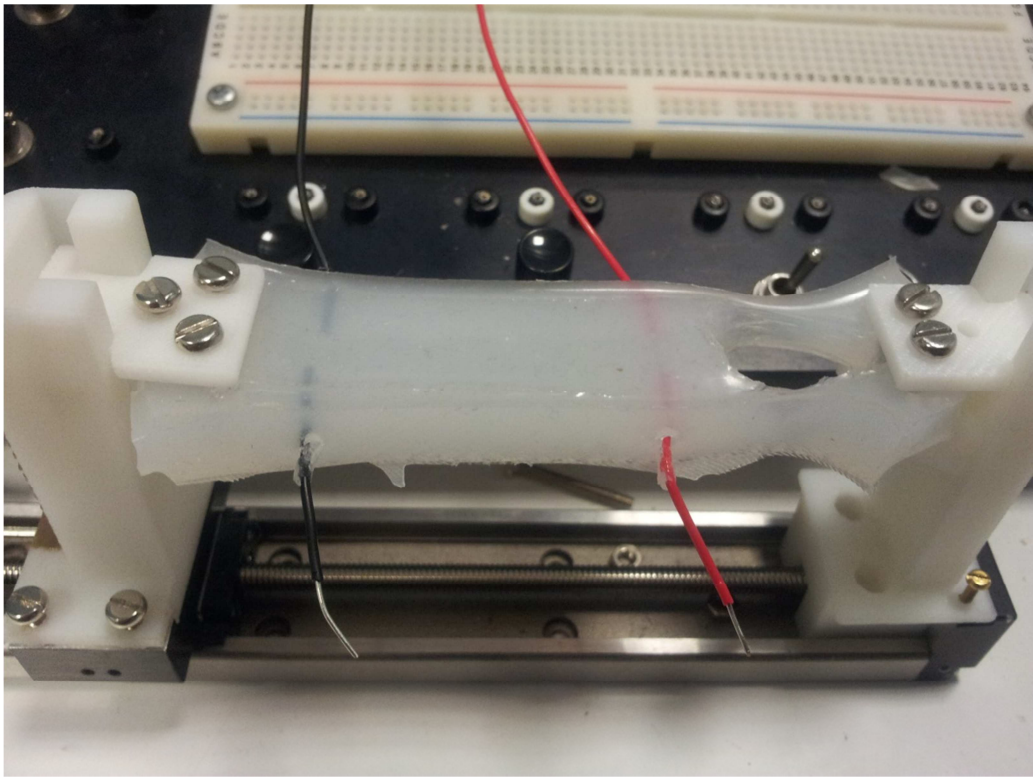

Figure 23: A view of the silicone sensor and its failure during the first experimental tensile test.

A Labview program is used for generating the supply of the sensor, through an analog output of NI DAQ board USB-6211. The generated signal was 500mV AC voltage with a frequency of 4kHz: changes in electrical resistance are then calculated from the measurement of the current generated at the electrodes.
The changes in the electrical resistance were then evaluated by applying axial strain. Each prototype was gradually stretched and data for each sensor were collected from 5 stretching tests, although the first was not used for analytical purpose because rubber-like materials exhibit a different behavior in their mechanical properties resulting from the first extension; this is known as the Mullins effect [66].

CHAPTER 4: EXPERIMENT

Proposed conductive embedded channel sensor was evaluated in the following sequences:

1) Alternate voltage is supplied through the electrodes;
2) A current is read out;
3) Fluid resistance changes are calculated with Ohm's law;
4) The data were analysed in Matlab

All tests are conducted at room temperature of around 25 ◦C.
The multimeter read a current and the resistance was then calculated as:

$$R = \frac{V_{RMS}}{I} \qquad (8)$$

where V_{RMS} is the root mean square of the sine wave and *I* is the read current, with the assumption that the impedance of the connection wires (conductivity much higher than saline) is negligible compared to the impedance of the saline solution inside the silicone channel.
When current flows in an ionic solution, both negative and positive ions are charged carriers so the resistivity of the solution is inversely proportional to the concentration. Different concentrations were evaluated, showing this principle.
The expected resistance of the filled channel was estimated as R = 100 Ω, but the measured one during each test was approximately five times larger due to the high resistance introduced by small air bubbles in the channel as they become an obstacle for the current flow.
Because of this, for a better comparison between tests, the results of each test have been offset by their initial resistance.
The presence of bubbles was a big issue during the first tests: the lateral hole through which the electrode is inserted becomes bigger during the stretching and thus leading small air bubble going inside the solution. Another problem was found in the excessive movements of the wires and their thickness that create unwanted changes in the length of the path of the current giving unstable measurements of the resistance.

4.1 Sensor characterizations

4.1.1 Stretching and compression response

As mentioned above, tensile tests were performed by imposing quasi static displacements from 0 to 35 mm with 1 mm step. In Figures 24 and 25 the average curve of the repeated tests is reported. In stretching mode the repeatability of the sensor was evaluated as the maximum variation between the measurements from different prototypes and it was found to be σ = ± 14.25 Ω, while in compression mode σ = ± 9 Ω.

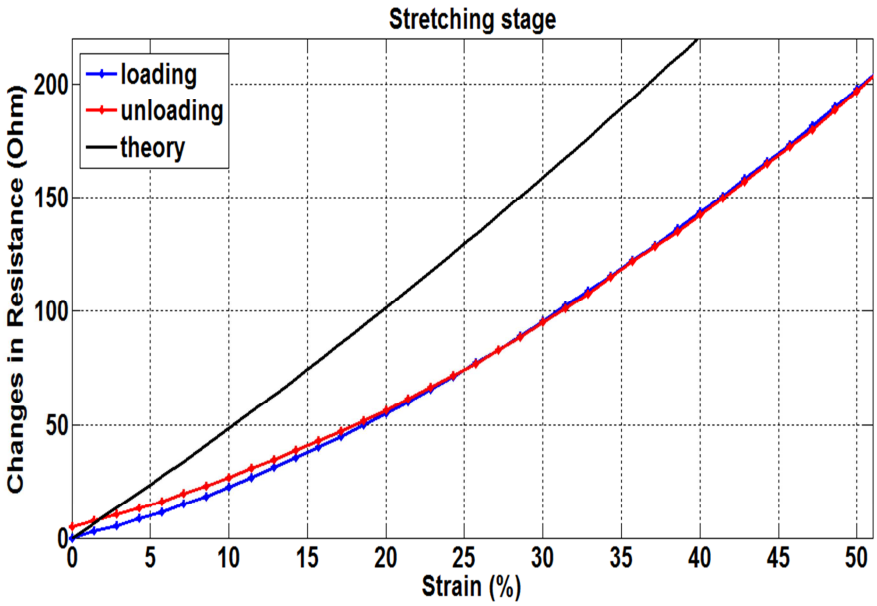

Figure 24. Experimental and theoretical results of changes in resistance are plotted versus strain.

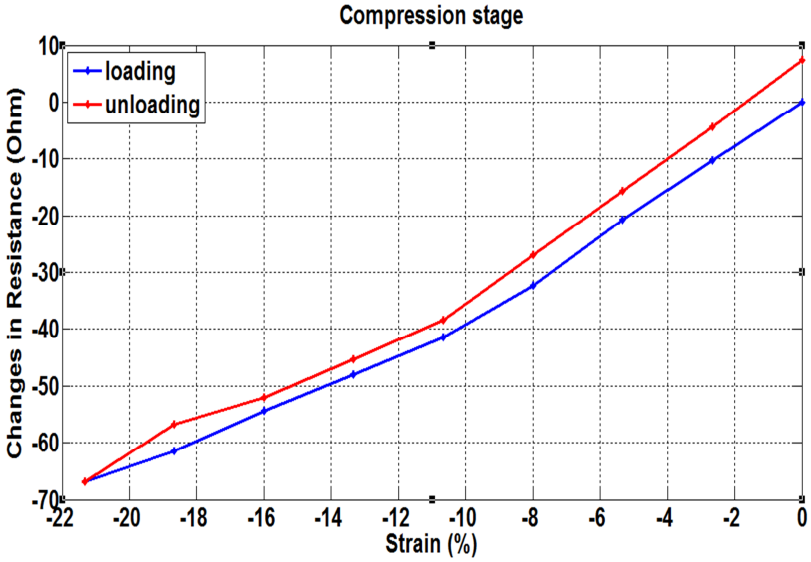

Figure 25. Loading and unloading data from the compression stage.

The sensor was calibrated for axial strain ranging from about -20 % to 50 %. Data from stretching and compression stages show similar behaviour and low hysteresis. Compression range from 0 to -20% shows decreasing of the electrical resistance, but after reaching approximately -20 % of strain, the device starts to bend, so increasing again its resistance; this problem could be avoided by mounting the sensor in pre-stretched form.

The stretching range goes from 0 to 50%. Even if bigger stretching are possible, the maximum value was limited due to the failure of the electrodes: in fact, during the stretching of the sensor the hole through which the electrodes were inserted became bigger, thus causing an increase in the presence of bubble inside the channel.

The results from the calibration tests contain an average of the data of 4 sensors from multiple loading and unloading stages for stretching and compression, to characterize and demonstrate the hysteresis, showing

good repeatability and little difference between the two curves (in Figures 24 and 25 , red and blue curves): for the stretching stage, the area of the hysteresis loop is 38.35 Ω, while the maximum hysteresis is 4.94 Ω and for the compression data they are respectively 25.34 Ω and 7.47 Ω.
The differences between the theoretical and the experimental curves and probably due to the slip of the sensor from the clamps and the elongation of the dead zone. The latter is the most likely reason, because the elongation of the silicone was not theoretically evaluated, while during the tests the clamps were holding the sensor starting from 4 mm before the edges of the channel.
The cross-sensitivity to pressure was very high, evaluated manually pressing the surface of the sensor during the stretching stage.

4.2 Results and discussion

The results showed good behaviour in strain sensing, with a reasonable approximation of the theoretical model; the signal was repeatable, with low hysteresis and strain ranging from approximately -20 % to 50 % even if bigger stretching values can be reached solving the issue of the electrodes.
The first tests also demonstrated some problems that must be solved: the sensitivity to pressure is an unwanted parameter as we want to measure only strain. Moreover, the air bubbles tend to affect the tests and the temporal stability of the sensor. A reason of the formation of the bubbles can be found in the presence of the thick electrodes that were also subjected to corrosion.

CHAPTER 5: SYSTEM IMPROVEMENTS

5.1 Geometry improvements

In pressure mode, Park, et al [53] used the linear elastic fracture mechanics (LEFM), considering that a vertical stress decreases the distance between the channel surfaces of quantity $\delta h = -\frac{2(1-v^2)wp}{E}$, neglecting the hydrostatic pressure, and derived a relationship for a channel embedded near the surface of the elastomer:

$$\Delta R = \frac{\rho L}{wh}\left\{\frac{1}{1-2(1-v^2)\frac{p}{p'}}-1\right\}, \qquad (9)$$

where *v* is Poisson's ratio, p is the applied pressure, p' is a characteristic pressure defined by p' = Eh/w, E is the Young's modulus, h/w is the aspect ratio (AR) of the channel.
Considering *v*=0.5 the equation becomes:

$$\frac{\Delta R}{R_0} = \frac{1}{1-\frac{3}{2}\frac{p}{p'}} - 1. \qquad (10)$$

It can be seen that the changes in the resistance strongly depend on the AR of the channel:

$$\frac{\Delta R}{R_0} = \frac{1}{\frac{2Eh}{3pw}-1}. \qquad (11)$$

In our case, the Young's modulus of the silicone rubber is 0.6 MPa, and considering to apply a force of about 2N, with a fingerprint area of 1cm^2, the total pressure to be applied is approximately 19 kPa; substituting in the previous equation:

$$\frac{\Delta R}{R_0} = \frac{1}{21\frac{h}{w}-1} \qquad (12)$$

We can plot (12), considering a known pressure of 19kPa.

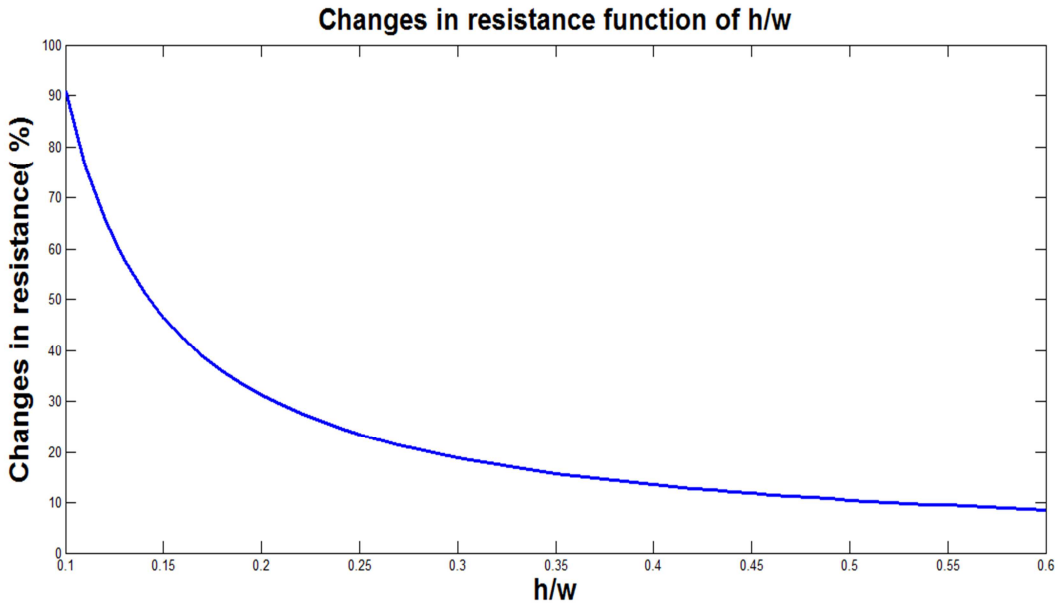

Figure 26. Changes in sensor resistance function of the aspect ratio of the channel section

As shown in Figure 26, the lower the aspect ratio of a rectangular microchannel, the greater the sensitivity of the sensor: the pressure required to produce an output signal can be increased by increasing the aspect ratio of the channels or implementing harder materials. So, depending on the ratio p/p', the relative electrical resistance can range from fractions of a percentage to one order of magnitude.
This means that for all applications, the design parameters E and h/w should be selected to know the relative resistance range and the input parameter range.
For our purpose we would like to measure only strain and not pressure so it would be preferable to have AR as big as possible: in the first feasibility studies, the channel AR was 0.25, while we need higher AR to only feel stretching. For this reason, the next geometry of the sensor should be with an AR=1.
Moreover, a cylindrical shape would be preferable, because it presents no corners and so less trapped bubbles and a better stresses uniform distribution.
In equation (5), Park et al replaced p with χp, where $\chi = \chi(x, z)$ is a correction depending on the relative position (x, z) of the channel (Figure 27). This is obtained by solving p using Boussinesq's [67] method and finding:

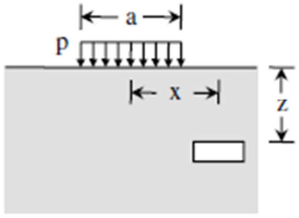

Figure 27. Scheme of the relative position of the channel inside the silicone

$$\chi = \frac{c1c2 - c3}{c4}$$

Where:

$$c1 = tan^{-1}\left(\frac{a + 2x}{2z}\right) + tan^{-1}\left(\frac{a - 2x}{2z}\right)$$

$$c2 = -8x^2a^2 + 32x^2z^2 + 8z^2a^2 + 16x^4 + 16z^4 + a^4$$

$$c3 = -16zax^2 + 4za^3 + 16z^3a$$

$$c4 = \pi(4x^2 + 4xa + a^2 + 4z^2)(4x^2 - 4xa + a^2 + 4z^2).$$

This is used to evaluate the change in electrical resistance as a function of *x* and *z*:

$$\frac{\Delta R}{R_0} = \frac{1}{\frac{2Eh}{3p\chi w} - 1}. \qquad (13)$$

As aforementioned, considering an applied force of 2N, with a fingerprint area of 1cm^2 (so a = 1cm) at a distance x = 0 from the centre of the channel, and substituting in the previous equation we obtain:

$$\frac{\Delta R}{R_0} = \frac{1}{21\frac{h}{\chi w} - 1} \qquad (14)$$

Considering the old rectangular geometry with AR=0.25, the changes in the electrical resistance as function of the channel depth z are shown in Figure 28. Instead, considering an AR=1 the percentage of changes in sensor electrical resistance are smaller.

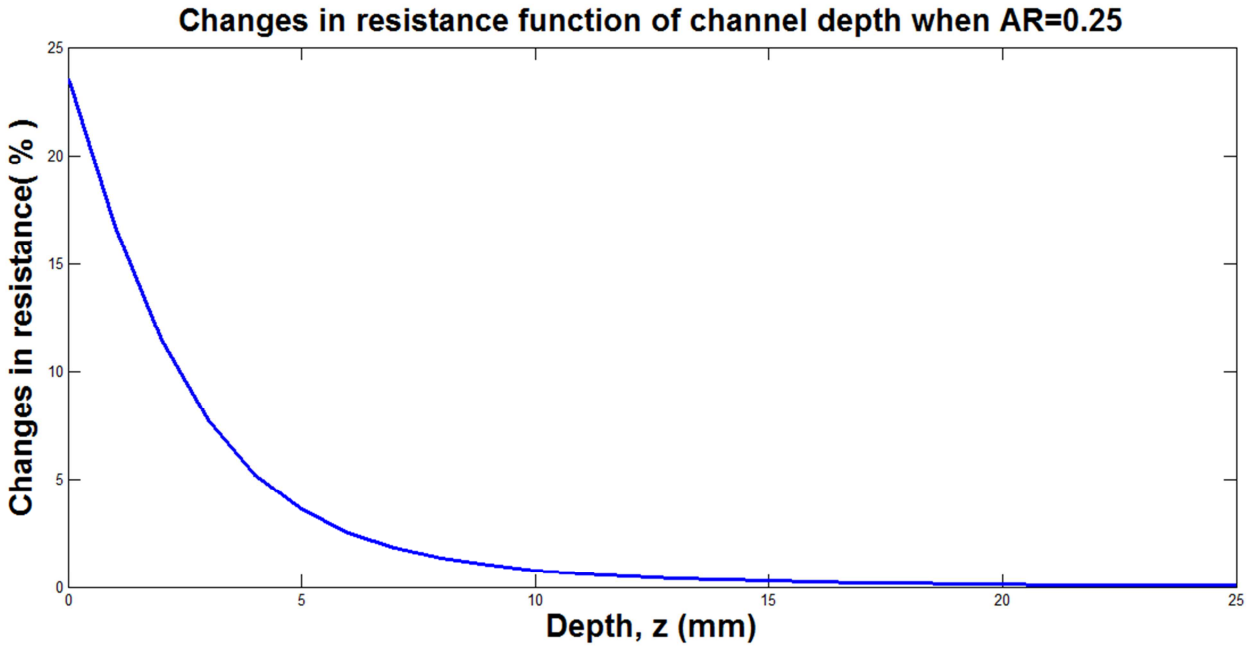

Figure 28. Percentage of changes in sensor electrical resistance function of channel depth when AR=0.25.

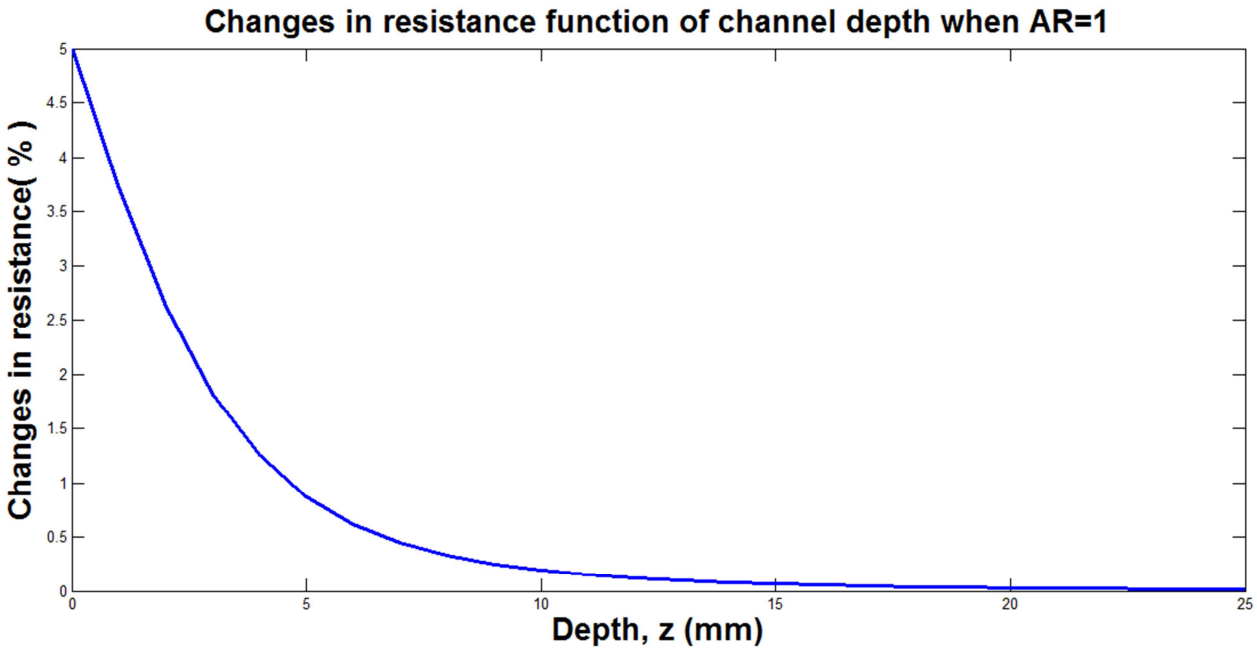

Figure 29. Percentage of changes in sensor electrical resistance function of channel depth when AR=1.

In stretching mode, for a circular cross-section and considering large deformations, when the channel is subject to stretch ε its radius *r* will change by:

$$\Delta r = r_f - r_0 = -r_0(1 - (1 + \varepsilon)^{-v}) \qquad (15)$$

Considering v = 0.5 and the maximum chamber elongation of the STIFF-FLOP robot $\varepsilon = 100\%$, we find:

$$r_f = 0.7 r_0$$

And the changes in resistance:

$$\Delta R = R_f - R_0 = \frac{\rho L_f}{\pi {r_f}^2} - \frac{\rho L_0}{\pi {r_0}^2} \propto \frac{1}{{r_0}^2} \qquad (16)$$

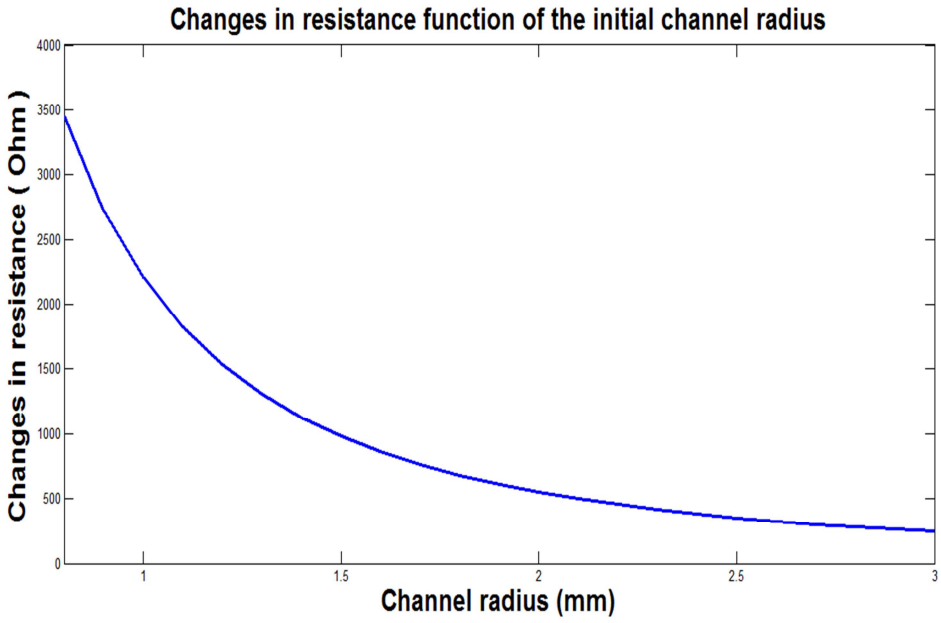

Figure 30. In stretching mode, changes in sensor electrical resistance function of the initial channel radius.

For these reasons, we choose as channel dimensions an initial length equal to the fluidic chamber one L_0 = 30 mm, a cylindrical geometry with an A/R = 1 and a section radius of 1 mm.

5.2 Air bubbles

Possible reasons of the air bubbles formation inside the liquid filled should be searched in:

- Gas permeability of the encapsulating polymer is high;
- Holes of the electrodes.

For improving the conductive solution, we mixed 75 % Glycerol with 25% NaCl solution; this dilution was chosen in order to prevent any undissolved NaCl crystals to be formed, and to obtain a more viscous solution for ease of fabrication. The glycerol is biocompatible and it prevents the formation of bubbles inside the channel, while reducing the gas permeability of the silicon.

5.3 Electrodes corrosion

The challenges were the dimension of the electrodes and their material, which was subjected to corrosion. We decide to produce electrodes as thin as possible, with a method called sputtering. During the sputtering, atoms are ejected from a source onto a substrate (in our case the silicone rubber), creating a film of 100nm of thickness, as shown in Figure 31. The sputtered metal was chosen to be gold, because it presents a very slow corrosion, and is biocompatible.

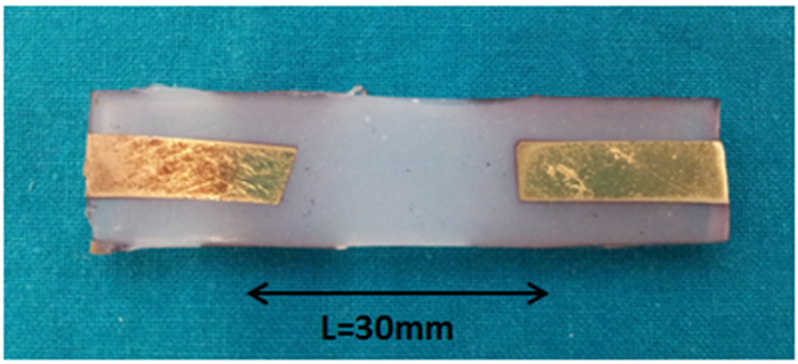

Figure 31. Section of the silicone sensor, presenting the sputtered electrodes

The most relevant issue was how the metal could follow the large deformations of the silicone rubber during the stretching of the sensor. Sputtering the metal directly on the substrate would create a thin and rigid film which would be destroyed during the first stretching of the sensor, as shown in Figure 32, thus not conducting the signal.

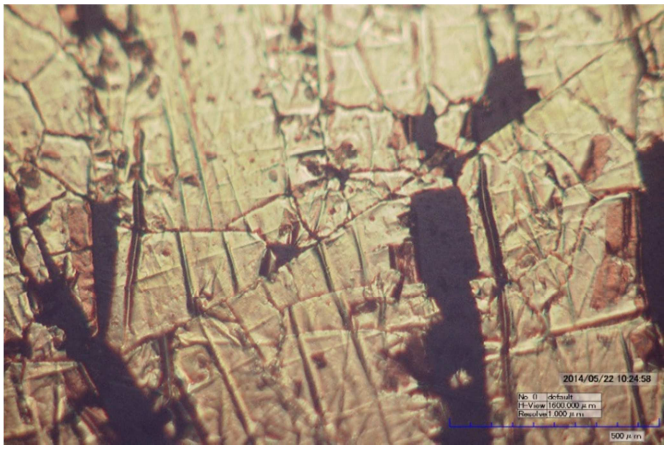

Figure 32. Microscope image of the sputtered electrode.

For this reason we decided to sputter the metal when the silicone was in pre-stretched form, in order to obtain a wrinkled structure when the rubber was released, that could follow the stretching of the sensor [68](Figure 33).

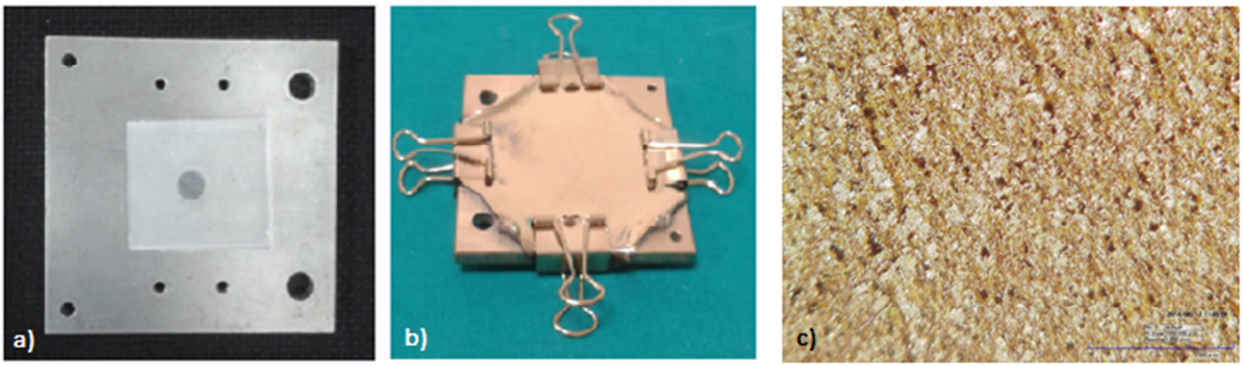

Figure 33. a) Silicone rubber before prestretching b) Silicone rubber after prestretching and sputtering of the metal c)Microscope view of the sputtered wrinkled electrode

CHAPTER 6: CONCLUSIONS AND FUTURE STUDIES

The present project lasted for approximately 8 months and was carried out between the BioRobotics Institute, Scuola Superiore Sant'Anna and the Centre for Robotics Research, King's College London. During this time, a review of the current devices in minimally invasive surgery was carried out; assessment of the state-of-art in soft sensing was subsequently conducted and demonstrated that existing solutions, while having the potential for bringing substantial advantages in soft devices, are currently not satisfactorily developed in term of stretchability, non-toxicity and biocompatibility. This is mainly because of lack of adequate performant biocompatible conductive fluids.

A promising, novel and alternative technique has therefore been developed and analysed. The proposed technique employs the use of saline solution for transmission of stretching signals. The high biocompatibility, low predicted costs and intrinsic simple design mean the technology devised may be suitable for most soft and flexible surgical devices. The theoretical analysis and the experimental validation of the sensor have been carried out with satisfactory results, giving inspirations for the system improvements.

The future developments of this novel technology could potentially contribute to make a fundamental stride in the field of soft and flexible devices. The expected future work is related to the improvement of the manufacturing method and on the testing characterizations of the new geometry, with the implementation and validation of the concepts.

Bibliography

1. Liang, R., *Optical Design for Biomedical Imaging.* SPIE press, 2010: p. 379-386.
2. V. Vitiello, S.L.L., T. P. Cundy, G.Z. Yang, *Emerging Robotic Platforms for Minimally Invasive Surgery.* IEEE REVIEWS IN BIOMEDICAL ENGINEERING, 2013. 6.
3. J. Lee, W.Y.C., *Advanced Developments in Neck Dissection Technique: Perspectives in Minimally Invasive Surgery.* Neck Dissection – Clinical Application and Recent Advances: p. 87-102.
4. E.-S. Hwang, J.S., Y.-J. Kim, *A Polymer-Based Flexible Tactile Sensor for Both Normal and Shear Load Detections and Its Application for Robotics.* JOURNAL OF MICROELECTROMECHANICAL SYSTEMS, 2007. 16(3): p. 556-563.
5. Sun D, W.C., Durrani A, King P, Cleary K, Wood B., *A Novel End-Effector Design for Robotics in Image Guided Needle Procedures.* The international journal of medical robotics + computer assisted surgery : MRCAS, 2006 March: p. 91-97.
6. Monaco, A., *The Next Generation-Smaller, lighter, and less expensive robots.* The institute, December 2012.
7. P. Puangmali, K.A., L. D. Seneviratne, D. Murphy, P. Dasgupta, *State-of-the-Art in Force and Tactile Sensing for Minimally Invasive Surgery.* IEEE SENSORS JOURNAL, NO. 4, APRIL 2008. 8.
8. T. Yoshikai, M.H., Y. Ishizaka, H. Fukushima, A. Kadowaki, T. Sagisaka, K. Kobayashi, I. Kumagai, M. Inaba, *Development of Robots with Soft Sensor Flesh for Achieving Close Interaction Behavior.* Advances in Artificial Intelligence, 2012. 2012: p. 27.
9. S. Tognarelli, M.S., G. Tortora, C. Quaglia, P. Dario, A. Menciassi, *An Endoluminal Robotic Platform for Minimally Invasive Surgery.* The Fourth IEEE RAS/EMBS International Conference on Biomedical Robotics and Biomechatronics Roma, Italy. June 24-27, 2012.
10. A. Loeve , P.B., J. Dankelman, *Scopes Too Flexible ...and Too Stiff.* IEEE PULSE, 2010. 1: p. 26-41.
11. Jayasingh, S.C., *Comparison of Advantages and Disadvantages between SILS and NOTES.* World Journal of Laparoscopic Surgery, 4(1), January-April 2011: p. 67-72.
12. G.P. Haber, M.A.W., R. Autorino, P. F. Escobar, M. D. Kroh, S. Chalikonda, R. Khanna, S. Forest, B. Yang, F. Altunrende, R. J. Stein, J. H. Kaouk, *Novel Robotic da Vinci Instruments for Laparoendoscopic Single-site Surgery.* Official journal of the société internationale d'urologie, 2010. 76 (6).
13. I. D. Walker, D.M.D., T. Flash, F. W. Grasso, R. T. Hanlon, B. Hochner, W. M. Kier, C. C. Pagano, C. D. Rahn, Q. M. Zhang, *Continuum Robot Arms Inspired by Cephalopods.*
14. L. Vyas, D.A., Kuo Chin-Hsing, J. S. Dai, P. Dasgupta, *Flexible Robotics.* BJU International, 2011. 107: p. 187-189.
15. T. Yoshikai, H.F., M. Hayashi, M. Inaba, *Development of Soft Stretchable Knit Sensor for Humanoids' Whole-body Tactile Sensibility.* 9th IEEE-RAS International Conference on Humanoid Robots December 7-10,2009 Paris, France.
16. D. Trivedi, C.D.R., W. M. Kier, I. D. Walker, *Soft robotics: Biological inspiration, state of the art, and future research.* Applied Bionics and Biomechanics, September 2008. 5(3): p. 99-117.
17. S. Kim, C.L., B. Trimmer, *Soft robotics: a bioinspired evolution in robotics.* Trends in Biotechnology, May 2013. 31(5).
18. M. Rolf, J.J.S., *Constant curvature continuum kinematics as fast approximate model for the Bionic Handling Assistant.* 2012 IEEE/RSJ International Conference on Intelligent Robots and Systems October 7-12, 2012. Vilamoura, Algarve, Portugal.
19. T. Mahl, A.H., O. Sawodny, *Forward Kinematics of a Compliant Pneumatically Actuated Redundant Manipulator.* 2012 7th IEEE Conference on Industrial Electronics and Applications (ICIEA).
20. W. McMahan, V.C., M. Csencsits, D. Dawson, I.D. Walker, B.A. Jones, M. Pritts, D. Dienno, M. Grissom, C.D. Rahn, *Field Trials and Testing of the OctArm Continuum Manipulator.* Proceedings of the 2006 IEEE International Conference on Robotics and Automation Orlando, Florida - May 2006.
21. K. Xu, R.E.G., J. Ding, P. K. Allen, D. L. Fowler, N. Simaan, *System Design of an Insertable Robotic Effector Platform for Single Port Access (SPA) Surgery.* The 2009 IEEE/RSJ International Conference on Intelligent Robots and Systems October 11-15,St. Louis, USA, 2009

22. T. Ota, A.D., D. Schwartzman, B. Zubiate, J. McGarvey, H. Choset, M. A. Zenati, *A Highly Articulated Robotic Surgical System for Minimally Invasive Surgery.* The Annals of Thoracic Surgery, April 2009. 87(4): p. 1253-1256.
23. D. Trivedi, C.D.R., W. M. Kier,I. D. Walker, *Soft robotics: Biological inspiration, state of the art, and future research.* Applied Bionics and Biomechanics, September 2008. 5(3): p. 99-117.
24. F. Lida, C.L., *Soft Robotics: Challenges and Perspectives.* Procedia Computer Science 7, 2011: p. 99-102.
25. T. Ranzani, M.C., G. Gerboni, I. De Falco, G. Petroni, A. Menciassi, *A modular soft manipulator with variable stiffness.* 3rd Joint Workshop on New Technologies for Computer/Robot Assisted Surgery, 11-12-13 September 2013, Verona, Italy.
26. K.Suzumori, S.E., T. Kanda, N. Kato, H. Suzuki, *A Bending Pneumatic Rubber Actuator Realizing Soft-bodied Manta Swimming Robot.* IEEE International Conference on Robotics and Automation, 2007: p. 4975-4980.
27. M. Cianchetti, T.R., G. Gerboni, I. De Falco, C. Laschi, A. Menciassi, *STIFF-FLOP Surgical Manipulator: mechanical design and experimental characterization of the single module* International Conference on Intelligent Robots and Systems (IROS), 2013: p. 3576-3581.
28. C. R. Wagner, N.S., R. D. Howe, *The Role Of Force Feedback In Surgery: Analysis Of Blunt Dissection.* The Tenth Symposium on Haptic Interfaces for Virtual Environment and Teleoperator Systems, March 24-25, 2002, Orlando.
29. H. Yousef, M.B., K. Althoefer, *Tactile sensing for dexterous in-hand manipulation in robotics-A review.* Sensors and Actuators A: Physical, 2011. 167(2): p. 171 - 187.
30. Dyer, S.A., *Wiley Survey of Instrumentation and Measurement*, ed. W.-I. Press. March 2004.
31. D.Walker, I., *Continuous Backbone "Continuum" Robot Manipulators.* ISRN Robotics, 2013.
32. S. Haddadin, M.S., S. Fuchs, T. Bodenmuller, A. Albu-Schaffer, G. Hirzinger, *Towards the Robotic Co-Worker.* Springer Tracts in Advanced Robotics, 2011. 70: p. 261-282.
33. A. M. Okamura, N.S., M. R. Cutkosky, *An Overview of Dexterous Manipulation.* Proceedings of the 2000 IEEE International Conference on Robotics & Automation San Francisco, CA April 2000: p. 255-262.
34. R. S. Dahiya, M.V., *Tactile sensing for robotic applications.* Sensors, Focus on Tactile, Force and Stress Sensors, 2008: p. 289-304.
35. R. J. Webster, B.A.J., *Design and Kinematic Modeling of Constant Curvature Continuum Robots: A Review.* The International Journal of Robotics Research, June 2010.
36. A. Bajo, N.S., *Finding Lost Wrenches: Using Continuum Robots for Contact Detection and Estimation of Contact Location.* 2010 IEEE International Conference on Robotics and Automation Anchorage Convention District May 3-8, 2010, Anchorage, Alaska, USA: p. 3666-3673.
37. C. Majidi, R.K.R.J.W., *A non-differential elastomer curvature sensor for softer-than-skin electronics.* Smart Mater. Struct., 2011.
38. T. C. Searle, K.A., L. Seneviratne, H. Liu, *An Optical Curvature Sensor for Flexible Manipulators.* IEEE International Conference on Robotics and Automation (ICRA), 2013 p. 4401-4405.
39. P.Polygerinos, A.A., T. Schaeffter, R. Razavi, L. D. Seneviratne, K. Althoefer, *MRI-Compatible Intensity-Modulated Force Sensor for Cardiac Catheterization Procedures.* IEEE TRANSACTIONS ON BIOMEDICAL ENGINEERING, MARCH 2011. 58(3): p. 721-726.
40. A. T. Tung, B.-H.P., D. H. Liang, G. Niemeyer, *Laser-Machined Shape Memory Alloy Sensors for Position Feedback in Active Catheters.* Sens Actuators A Phys. 2008 September 15: p. 83–92.
41. D. P. J. Cotton, I.M.G., S. P. Lacour, *A Multifunctional Capacitive Sensor for Stretchable Electronic Skins.* IEEE SENSORS JOURNAL, DECEMBER 2009. 9(12).
42. M.A. Lacasse, V.D., C. Gosselin, *Characterization of the Electrical Resistance of Carbon-Black-Filled Silicone: Application to a Flexible and Stretchable Robot Skin.* IEEE International Conference on Robotics and Automation Anchorage Convention District May 3-8, 2010, Anchorage, Alaska, USA, 2010.

43. H.-K. Lee, J.C., S.-Il Chang, E. Yoon, *Normal and Shear Force Measurement Using a Flexible Polymer Tactile Sensor With Embedded Multiple Capacitors.* JOURNAL OF MICROELECTROMECHANICAL SYSTEMS, AUGUST 2008. 17(4): p. 934-942.
44. T. Hoshi, H.S., *Robot Skin Based on Touch-Area-Sensitive Tactile Element* Proceedings of the 2006 IEEE International Conference on Robotics and Automation Orlando, Florida, May 2006: p. 3463-3468.
45. K. Noda, E.I., K. Matsumoto, I. Shimoyama, *Stretchable liquid tactile sensor for robot-joints.* 2010 IEEE International Conference on Robotics and Automation Anchorage Convention District May 3-8, 2010.
46. M. Segev-Bar, A.L., M. Nir-Shapira, G. Shuster, H. Haick, *Tunable Touch Sensor and Combined Sensing Platform: Toward Nanoparticle-based Electronic Skin.* ACS Applied Materials & Interfaces, 2013. 5: p. 5531-5541.
47. *http://www.pressureprofile.com/products-tactarray*.
48. F. Lorussi, E.P.S., M. Tesconi, A. Tognetti, D. De Rossi, *Strain sensing fabric for hand posture and gesture monitoring.* IEEE Transactions on Information Technology in BioMedicine. 9(3): p. 372-381.
49. M.-Y. Cheng, C.-M.T., Y.-Z. Lai, Y.-J. Yang, *The development of a highly twistable tactile sensing array with stretchable helical electrodes.* Sensors and Actuators: A Physical 2011. 166: p. 226 - 233.
50. J. Ulmen, M.C., *A Robust, Low-Cost and Low-Noise Artificial Skin for Human-Friendly Robots.* IEEE International Conference on Robotics and Automation (ICRA), 2010: p. 4836-4841.
51. Y.-L. Park, S.C.R., R. J. Black, K. K. Chau, B. Moslehi, M. R. Cutkosky, *Exoskeletal Force-Sensing End-Effectors With Embedded Optical Fiber-Bragg-Grating Sensors.* IEEE TRANSACTIONS ON ROBOTICS, 2009. 24(6): p. 1319-1331.
52. K. Noda, K.H., K. Matsumoto, I. Shimoyama, *A shear stress sensor for tactile sensing with the piezoresistive cantilever standing in elastic material.* Sensors and Actuators A: Physical, 2006. 127(2): p. 295–301.
53. Y.L. Park, C.M., R. Kramer, P. Bérard, R. J. Wood, *Hyperelastic pressure sensing with a liquid-embedded elastomer.* J. Micromech. Microeng., 2010.
54. Y.L. Park, B.R.C., R. J. Wood, *Design and Fabrication of Soft Artificial Skin Using Embedded Microchannels and Liquid Conductors.* IEEE SENSORS JOURNAL, AUGUST 2012. 12(8,).
55. R. K. Kramer, C.M., R. Sahai, R. J. Wood, *Soft Curvature Sensors for Joint Angle Proprioception.* IEEE/RSJ International Conference on Intelligent Robots and Systems September 25-30, 2011. San Francisco, CA, USA, 2011.
56. R. K. Kramer, C.M., R. J. Wood, *Wearable Tactile Keypad with Stretchable Artificial Skin.*
57. P. Roberts, D.D.D., W. Shan, T. Lu, C. Majidi, *Soft-Matter Capacitive Sensor for Measuring Shear and Pressure Deformation.* IEEE International Conference on Robotics and Automation (ICRA)2013: p. 3529-3534.
58. M. D. Dickey, R.C.C., R. J. Larsen, E. A. Weiss, D. A. Weitz, G. M. Whitesides, *Eutectic Gallium-Indium (EGaIn): A Liquid Metal Alloy for the Formation of Stable Structures in Microchannels at Room Temperature.* Advanced Functional Materials, April 11, 2008. 18(7): p. 1097-1104.
59. S. Rodrigues, M.D., C. R. López, A. Grenha, *Biocompatibility of Chitosan Carriers with Application in Drug Delivery.* Journal of Functional Biomaterials, 2012: p. 615-641.
60. A. H. Gosline, V.A., A. Kassam, P. E. Dupont, *Achieving Biocompatibility in Soft Sensors for Surgical Robots.* The Hamlyn Symposium on Medical Robotics, 2013.
61. Y.-N. Cheung, Y.Z., C.-H. Cheng, C. Chao,WallaceWoon-Fong Leung, *A novel fluidic strain sensor for large strain measurement.* Sensors and Actuators A: Physical, 2008: p. 401-408.
62. D. Prasad, A.K.S., H.C. Sharma, *Electric Shock and Human Body.* International Journal of Electrical and Power Engineering, 2010. 4(3): p. 177-181.
63. *http://srdata.nist.gov/solubility/index.aspx*.
64. *http://www.slb.com/*.
65. J. C. Lotters, W.O., P. H. Veltink, P. Bergveld, *The mechanical properties of the rubber elastic polymer polydimethylsiloxane for sensor applications.* J. Micromech. Microeng, 1997. 7: p. 145–147.

66. J. Diani, B.F., P. Gilormini, *A review on the Mullins effect.* European Polymer Journal, 2009. 45: p. 601–612.
67. Anderson, T.L., *Theory of Elasticity 3rd edn*, ed. McGraw-Hill. 2005.
68. M. Cianchetti, V.M., B. Mazzolai, C. Laschi, P. Dario, *A new design methodology of electro-strictive actuators for bio-inspired robotics.* Sensors and Actuators B: Chemical, 2009: p. 288-297.